

pubs.acs.org/JACS Article

# Linking Molecular Behavior to Macroscopic Properties in Ideal Dynamic Covalent Networks

Bruno Marco-Dufort, Ramon Iten, and Mark W. Tibbitt\*



Cite This: J. Am. Chem. Soc. 2020, 142, 15371-15385



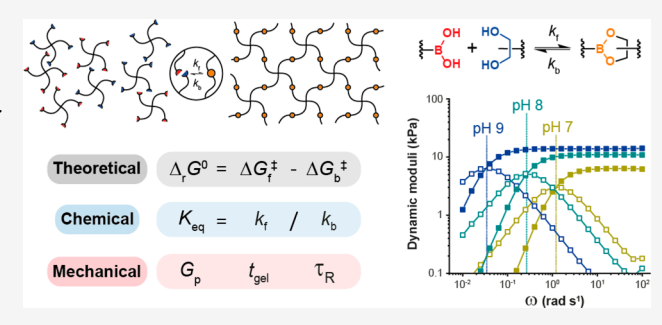
**ACCESS** 

Metrics & More

Article Recommendations

Supporting Information

ABSTRACT: Dynamic covalent networks (DCvNs) are increasingly used in advanced materials design with applications ranging from recyclable thermosets to self-healing hydrogels. However, the relationship between the underlying chemistry at the junctions of DCvNs and their macroscopic properties is still not fully understood. In this work, we constructed a robust framework to predict how complex network behavior in DCvNs emerges from the chemical landscape of the dynamic chemistry at the junction. Ideal dynamic covalent boronic ester-based hydrogels were used as model DCvNs. We developed physical models that describe how viscoelastic properties, as measured by shear rheometry, are linked



to the molecular behavior of the dynamic junction, quantified via fluorescence and NMR spectroscopy and DFT calculations. Additionally, shear rheometry was combined with Transition State Theory to quantify the kinetics and thermodynamics of network rearrangements, enabling a mechanistic understanding including preferred reaction pathways for dynamic covalent chemistries. We applied this approach to corroborate the "loose-bolt" postulate for the reaction mechanism in Wulff-type boronic acids. These findings, grounded in molecular principles, advance our understanding and rational design of dynamic polymer networks, improving our ability to predict, design, and leverage their unique properties for future applications.

# **■ INTRODUCTION**

Dynamic covalent chemistry has emerged as an elegant molecular design strategy to engineer functional polymer networks that combine advantageous properties of both chemically and physically cross-linked materials. In this approach, covalent bonds that break and form reversibly on experimental time scales are installed in the backbone of dynamic covalent networks (DCvNs), enabling stress relaxation and material flow through bond exchange. In general, the binding affinity and kinetics of the dynamic covalent chemistry are sensitive to exogenous properties such as temperature, pH, and light. Thus, subtle shifts in environmental conditions can transform the material reversibly from a network to a melt and back again, allowing for self-healing, as well as shaping and reforming. That is, DCvNs form stable networks, which are also easy to process.

Examples of DCvNs include robust yet recyclable vitrimers, based on epoxy resins, which were designed using controlled cross-link rearrangement via temperature induced transesterification.<sup>3</sup> In another approach, Diels—Alder (DA) cycloaddition enabled thermal self-healing of cross-linked polymer networks; subsequent application of heat resulted in network flow via the retro-DA reaction.<sup>4</sup> Light and pH have also been exploited to modulate reversible networks through the formation and cleavage of disulfide bonds.<sup>5</sup> Further, dynamic covalent bond exchange can occur under mild, aqueous conditions without catalysts. Boronic esters, for

example, have formed dynamic covalent hydrogels that have been leveraged as responsive drug delivery systems, dynamic scaffolds for cell culture, and for sensing of cis-diol-containing biomolecules. <sup>6–9</sup>

In each case, the dynamic properties of the DCvN, e.g., gel point, plateau modulus, and relaxation time, emerge from the molecular behavior of the dynamic covalent chemistry installed at the network junctions.<sup>2</sup> This stands in contrast to permanent covalent polymer networks, which are engineered via network topology, e.g., polymer molecular weight, branching and functionality, and/or concentration.<sup>10</sup>

In order to predict the dynamic properties of adaptable networks, early theoretical frameworks employed the hindered reptation model, where the successive breaking of only a few cross-links allows interacting polymer chains to diffuse along their confined "tubes". Semenov and Rubinstein pioneered this approach to relate bond kinetics and relaxation behavior in associating polymers. This framework was extended by Sheridan and Bowman to establish a relationship between the

Received: June 8, 2020 Published: August 18, 2020





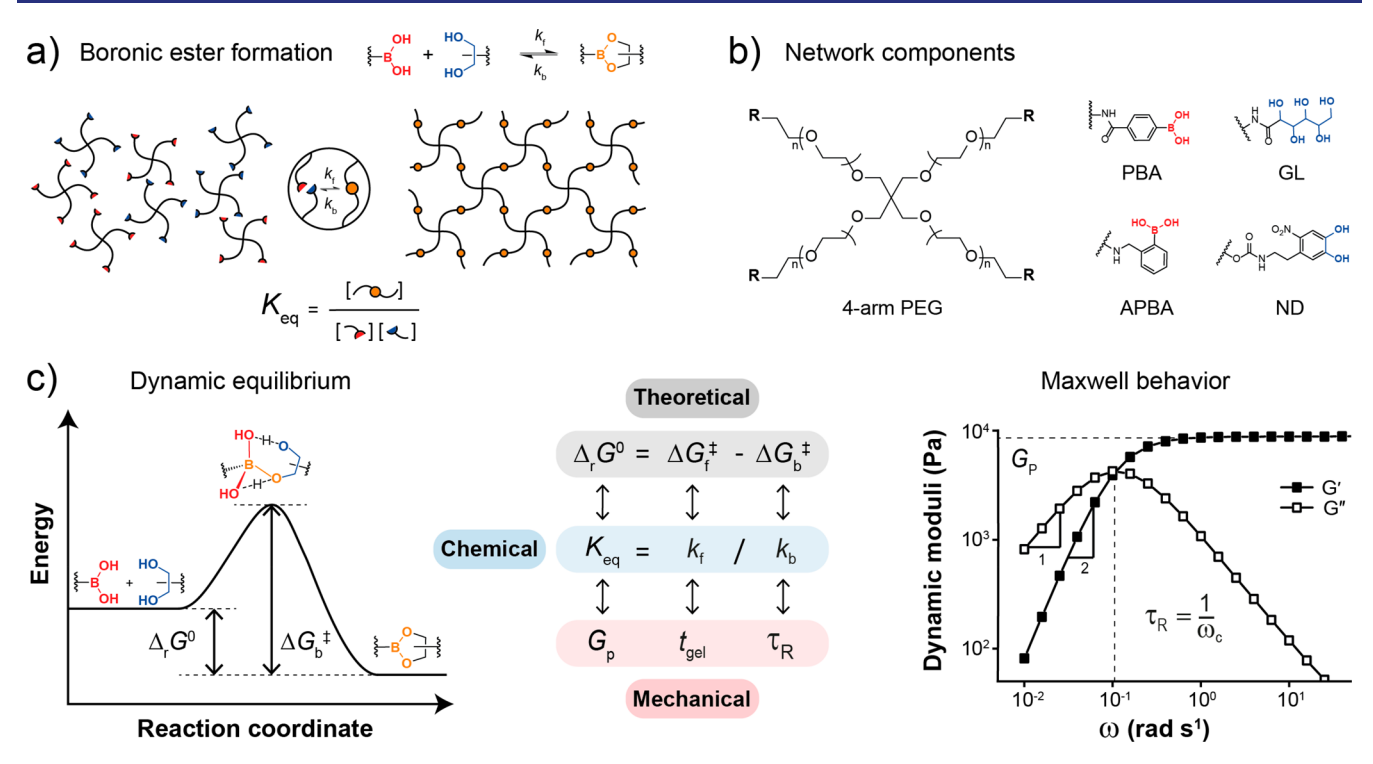


**Figure 1.** Molecular behavior controls macroscopic properties in ideal dynamic covalent networks (DCvNs). (a) Boronic ester-based hydrogels formed via reversible covalent bonding between boronic acid (red) and diol (blue), forming dynamic boronic esters (orange). (b) 4-arm poly(ethylene glycol) (PEG) macromers (10000 g mol<sup>-1</sup>) were end-functionalized with either a boronic acid (PBA or APBA) or with a diol (GL or ND). (c) Boronic ester-based networks exhibited canonical Maxwell model behavior with a well-defined plateau modulus,  $G_p$ , and a relaxation time,  $\tau_R$  (PEG-PBA/GL, pH 8, 10 wt %;  $\gamma = 1\%$ ). In a dynamic covalent system, the reactants and the products are in dynamic chemical equilibrium, as defined by the equilibrium constant for the reaction,  $K_{eqv}$  which is related to the reaction Gibbs free energy,  $\Delta_r G^\circ$ . The kinetics of the system depend on the size of the energetic barrier needed to access the transition states, which is defined by the activation Gibbs free energies,  $\Delta G_f^{\ddagger}$  and  $\Delta G_b^{\ddagger}$ . The rheological properties of the gels ( $G_p$ ,  $t_{gel}$ ) and  $\tau_R$ ) were linked to the microscopic parameters characterizing the dynamic junction ( $K_{eqv}$  and the forward and backward reaction rates,  $k_f$  and  $k_b$ ), which were quantified via a fluorescence-based spectroscopy assay, NMR spectroscopy, and DFT calculations.

viscoelastic properties of a thermoreversible DA network and its chemical structure.<sup>14</sup> While these models form the foundation for understanding dynamic covalent networks, less emphasis has been placed on how modifications in the reaction mechanism of the dynamic chemistry, which can occur with changes in environmental conditions, e.g., pH, temperature, or mechanical stress, impact the final mechanical properties of the formed network.

Indeed, the specific chemistry installed at the dynamic crosslink significantly influences the properties of DCvNs. <sup>9,15</sup> The thermodynamics and kinetics of bond formation, cleavage, and reformation, define the dynamics of network strand rearrangement and the time scales for stress relaxation and healing. Therefore, the design and application of DCvNs require a precise understanding of how the molecular behavior of the dynamic chemistry, and environmental conditions, dictate emergent macroscopic properties of the network.

The connection between bond chemistry and material properties was recognized by Craig and co-workers, who demonstrated that the rate-determining step for the mechanical response in coordinatively cross-linked gels was the small molecule dissociation rate of the cross-links. Similar scaling was observed in boronic ester-based networks; the rate of self-healing was correlated to the rate of boronic transesterification, which was tuned via neighboring effects over several orders of magnitude. Nevertheless, a larger question remains: how is complex network behavior in DCvNs controlled by the local

chemical landscape and environmental conditions of the dynamic linkages? Addressing this presents major challenges, as the exploration of structure—function relationships within DCvNs can be hindered by the presence of defects and other nonidealities. Their influence on the macroscopic properties is difficult to differentiate from that of the underlying chemistry.

Therefore, in this work, we developed a robust framework to predict how complex macroscopic properties in DCvNs emerge from the chemical landscape of the dynamic chemistry at the junction. Our approach was centered on the use of ideal networks, whose controlled and homogeneous structures improve the resolution of rheological analyses. 18,19 We selected ideal dynamic covalent boronic ester-based hydrogels as model DCvNs (Figure 1a). The complex properties of boronic esterbased DCvNs are regulated by pH, temperature, and the specific functionality of the boronic acid-diol binding pair (Figure 1b). 20,21 These additional degrees of freedom allowed us to systematically explore the effect of the chemical environment on network behavior. We applied the principles of physical organic chemistry to relate viscoelastic properties, as measured by shear rheometry, to the kinetics and thermodynamics of the dynamic junction, quantified via fluorescence-based spectroscopy, NMR spectroscopy, and Density Functional Theory (DFT) calculations (Figure 1c).

After characterizing the system at both the molecular and macroscopic level, we developed physical models to describe how complex viscoelasticity in these networks arises from the

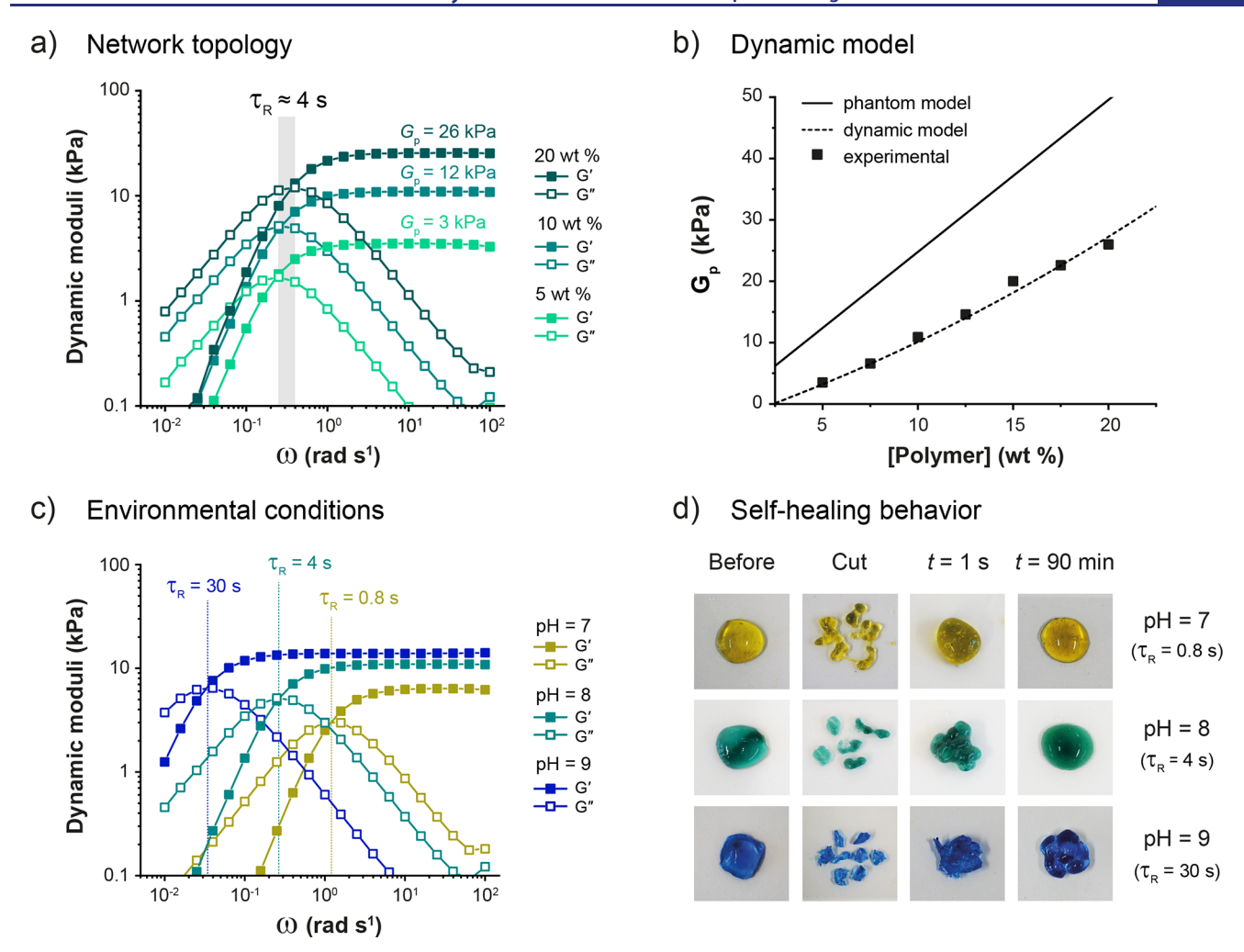


Figure 2. Network topology and environmental conditions modulate properties in boronic ester-based networks. (a) The plateau modulus,  $G_{\rm p}$ , varied with the polymer content (wt %) of the gels (PEG-PBA/GL, pH 8;  $\gamma=1$ %). (b)  $G_{\rm p}$  for PEG-PBA/GL was fit to our dynamic phantom network model as a function of polymer concentration (wt %) with  $K_{\rm eq}=275\pm35$  (pH 8;  $\gamma=1$ %). The dynamic model is a modification of the classic phantom network model for ideal networks that accounts for the modulation of formed cross-links based on  $K_{\rm eq}$  and the concentration of reactive groups, c. (c) pH influenced the relaxation time,  $\tau_{\rm R}$  (PEG-PBA/GL, 10 wt %;  $\gamma=1$ %). (d) Self-healing behavior in the gels at different pH scaled with  $\tau_{\rm R}$ , as bond rearrangement restored network connectivity (PEG-PBA/GL, 10 wt %).

chemical landscape at the cross-links. Shear rheometry was combined with Transition State Theory to investigate the thermodynamics and kinetics of the network rearrangements (Figure 1c). This enabled a mechanistic understanding of cross-link chemistry, including quantitative activation energies, directly from viscoelastic measurements. Importantly, we demonstrate that rheometric measurements of ideal DCvNs can be leveraged as a spectroscopic tool to elucidate reaction pathways for dynamic covalent chemistries, and our findings corroborated the "loose bolt" internal conversion postulate for Wulff-type boronic acids.<sup>22</sup>

# ■ RESULTS AND DISCUSSION

Ideal Boronic Ester-Based Dynamic Covalent Networks (DCvNs) Exhibit Canonical Maxwell Model Viscoelasticity. Ideal dynamic covalent hydrogels were fabricated via boronic ester formation from 4-arm poly-(ethylene glycol) (PEG) macromers ( $M_{\rm n} \approx 10000~{\rm g~mol}^{-1}$ ), end-functionalized with phenylboronic acid (PBA) derivatives or *cis*-1,2-diol containing moieties. Robust hydrogels formed quickly ( $\approx 1$ –10 s) after mixing equimolar amounts of PEG-PBA and PEG-diol. Four different boronic ester cross-links

were investigated, by combining PBA derivatives (PEG-PBA or PEG-APBA) with diol moieties (PEG-GL or PEG-ND) (Figure 1b and SI Section 3).

Parada and Zhao demonstrated that ideal reversible networks, formed via dynamic cross-linking of low and equal molecular weight polymer chains, behave as single Maxwell elements. <sup>19,23</sup> Throughout this work, we use the term ideal to describe the polymer networks formed from simple 4-arm PEG precursors, resulting in defined lengths of elastically active network strands as well as homogeneous cross-link functionality and network architecture. In our work, the DCvNs exhibited canonical Maxwell model behavior, supporting the formation of ideal networks. The storage modulus,  $G'(\omega)$ , and the loss modulus,  $G''(\omega)$ , scaled as  $G'(\omega) \propto \omega^2$  and  $G''(\omega) \propto \omega^1$  at low  $\omega$ , following standard scaling for terminal relaxation in the Maxwell model (Figure 1c and SI Section 6.1).

The plateau modulus,  $G_p$ , of these well-defined networks was determined by the concentration of elastically active chains (as there were few defects or chain entanglements), <sup>24</sup> while the relaxation time,  $\tau_R$ , depended on the dynamics of the reversible cross-links (as the Rouse relaxation time of the chains was much shorter than the dissociation time of the reversible cross-

link).<sup>25</sup> The relaxation time,  $\tau_R = 1/\omega_c$  represented the transition between elastic behavior, at high  $\omega$ , and viscous behavior, at lower  $\omega$ , where  $\omega_c$  is the crossover frequency when  $G'(\omega) = G''(\omega) = G_p/2$ .<sup>26,27</sup>

 $K_{eq}$  Predicts  $G_p$  through the Dynamic Phantom Network Model. In the PEG-PBA/GL system,  $G_p$  increased monotonically with polymer concentration (Figure 2a), consistent with classic rubber elasticity (phantom network model; eq 1)<sup>27</sup>

$$G_{p,phantom} = (\nu - \mu)RT \tag{1}$$

where  $\nu$  and  $\mu$  are the concentrations of elastically active network strands and cross-links, respectively.

 $G_{\rm p}$  was predicted for the PEG-PBA/GL networks (pH 8) by modifying the phantom network model to account for the dynamic nature of the boronic ester bonds (Figure 2b). As the cross-links break and reform on experimental time scales,  $\nu$  and  $\mu$  vary with the fraction of formed cross-links, or conversion, p (see SI Section 6.2 for a full description of our model).  $^{19,28,29}$  At equilibrium, p can be calculated from the concentration of functional groups, c, and the equilibrium constant,  $K_{\rm eq}$  (eq 2).  $^{19,28}$ 

$$p = \left(1 + \frac{1}{2cK_{\rm eq}}\right) - \left[\left(1 + \frac{1}{2cK_{\rm eq}}\right)^2 - 1\right]^{1/2}$$
 (2)

Equation 2 formed the basis of the dynamic phantom network model. Further, when combined with the Flory–Stockmayer Theory, it defined a critical equilibrium constant,  $K_{\rm eq,c}$  for network formation  $(p>p_c)$ . For a network formed from tetra-functional macromers,  $c \cdot K_{\rm eq} \geq 3/4$ , which indicates  $K_{\rm eq,c} = 18.75$  when c = 0.04 M (10 wt % PEG;  $M_{\rm n} \approx 10000$  g mol<sup>-1</sup>).

By the fitting of the dynamic model to the experimental values of  $G_{\rm p}$ ,  $K_{\rm eq}$  was determined to be 275  $\pm$  35. At the same pH,  $K_{\rm eq}$  was measured by fluorescence to be 440  $\pm$  140 (SI Section 5.3), orresponding to  $G_{\rm p}$  = 14.3  $\pm$  1.5 kPa (10 wt % PEG-PBA/GL). For comparison,  $G_{\rm p}$  = 12.0  $\pm$  0.6 kPa by shear rheometry (Table 1).  $K_{\rm eq}$  was also calculated from 1D  $^{1}{\rm H}$ 

Table 1. Experimental Relations between Molecular Behavior at the Junction and Macroscopic Properties

Method <sup>a</sup>	$\Delta_r G^0$ (kJ mol <sup>-1</sup> )	$K_{ m eq}$	$G_p$ (kPa)
Rheology	$-13.9 \pm 0.3$	$275 \pm 35$	$12.0 \pm 0.6$
Fluorescence	$-15.1 \pm 0.9$	$440 \pm 140$	$14.3 \pm 1.5$
NMR	$-13.9 \pm 0.3$	$277\pm37$	$12.1 \pm 0.7$
DFT	-14.3	323	12.9

 $^{\prime\prime}K_{\rm eq\prime}$   $G_{\rm p\prime}$  and  $\Delta_{\rm r}G^{\circ}$  were determined for the PEG-PBA/GL system (pH 8, 10 wt %) by molecular spectroscopy (fluorescence and  $^{1}{\rm H}$  NMR), rheology, and DFT, respectively. Values that were measured directly are highlighted in bold. The rest of the values were converted from the values in bold using eqs 2 and 3. All experimental measurements are reported as triplicates with the mean  $\pm$  standard deviation.

NMR spectroscopy (SI Section 5.4) and DFT calculations, based on the reaction Gibbs free energy (eq 3; SI Section 5.1).

$$\Delta G_{\rm r}^0 = -RT \ln K_{\rm eq} \tag{3}$$

 $K_{\rm eq}$  was quantified as 277  $\pm$  37 from NMR and 323 from DFT, corresponding to  $G_{\rm p}$  = 12.1  $\pm$  0.7 and 12.9 kPa, respectively.

Our approach to quantify the equilibrium constant of the binding pair experimentally, via fluorescence spectroscopy, NMR, and DFT, predicted the plateau modulus,  $G_{\rm p}$ , in DCvNs with near quantitative agreement. For reference, we observed  $K_{\rm eq}$  values from  $10^0$  to  $10^5$  for the DCvNs studied here. The agreement with the dynamic phantom network model confirmed the ideal nature of these gels. In the sections below, ideal networks were critical to explain complex macroscopic properties based on the chemical landscape of the dynamic covalent chemistry, without confounding effects from network defects. Further, the accurate estimation of  $G_{\rm p}$  from molecular measurements demonstrated the predictive power of the dynamic model framework.

Environmental Conditions Regulate Stability and Dynamics in DCvNs. The environmental conditions altered the properties of the emergent networks. As boronic esters are under thermodynamic control (dynamic chemical equilibrium),  $K_{\rm eq}$  and the number of formed cross-links varied with pH and temperature. Thus, the tuning of  $K_{\rm eq}$  provided a direct handle to modulate  $G_{\rm p}$  in these DCvNs. To a first approximation, the equilibrium of boronic ester formation shifts toward the products (higher  $K_{\rm eq}$ ) under basic conditions. Under more acidic conditions, the reactants are favored (lower  $K_{\rm eq}$ ). According to our dynamic model (SI Section 6.2), this implies that networks should be more stable at higher pH, as was observed in the PEG-PBA/GL system (10 wt % PEG);  $G_{\rm p}$  was significantly higher at pH 9 (13 kPa) as compared with pH 7 (6 kPa) (Figure 2c).

The dynamics of the boronic ester-based hydrogels, as measured by  $\tau_R$ , were also heavily influenced by the environmental conditions;  $\tau_R$  varied by 2 orders of magnitude over a narrow pH window (pH 7–9; Figure 2c). Furthermore, after being cut into small pieces, the DCvNs were able to fully heal. The time for self-healing scaled with  $\tau_R$  at each pH, as network connectivity was restored through bond rearrangement (Figure 2d and SI Section 7.1).  $\tau_R$  provides a direct link between the bulk properties of DCvNs and the molecular behavior at the junctions. Semenov and Rubinstein established that  $\tau_R$  scales with the lifetime of the bond,  $\tau_B = 1/k_b$ , where  $k_b$  is the dissociation rate constant of the cross-link (eq 4). 14

$$\tau_{\rm R} \propto \tau_{\rm B} = \frac{1}{k_{\rm b}} \tag{4}$$

To support the validity of this model, we estimated  $k_{\rm f}$  and  $k_{\rm b}$  for PBA in the presence of a diol (fructose) via 2D <sup>1</sup>H NMR EXSY measurements (Figure 3a; SI Section 5.5). <sup>17</sup> Our data corroborated the seminal work by Craig and co-workers, where the rheological data were renormalized to the small molecule  $k_{\rm b}$  of organometallic cross-links. <sup>16</sup> In our system, the boronic ester-based DCvNs also exhibited time-cross-link superposition; the relaxation times from the frequency sweeps at pH 7, 8, and 9 (shown in Figure 2c) were superimposed when scaled by  $k_{\rm b}$ ' measured at each pH (Figure 3b). Conversely,  $G_{\rm p}$  at pH 7, 8, and 9 did not overlap because  $G_{\rm p}$  depends on  $K_{\rm eq}$  and not on the kinetics at the junction. The scaling of the boronic ester dissociation rates with the bulk relaxation time of the material confirmed that  $\tau_{\rm R}$  in our system is directly related to the cross-linking dynamics of the junction, as expected from eq 4.

These results confirmed previous experimental observations of boronic ester-based hydrogels,  $^{17,19,20,28,32}$  namely, that  $\tau_R$  is highly dependent on the local chemical environment of the junction (Figure 3), while being relatively unaffected by the

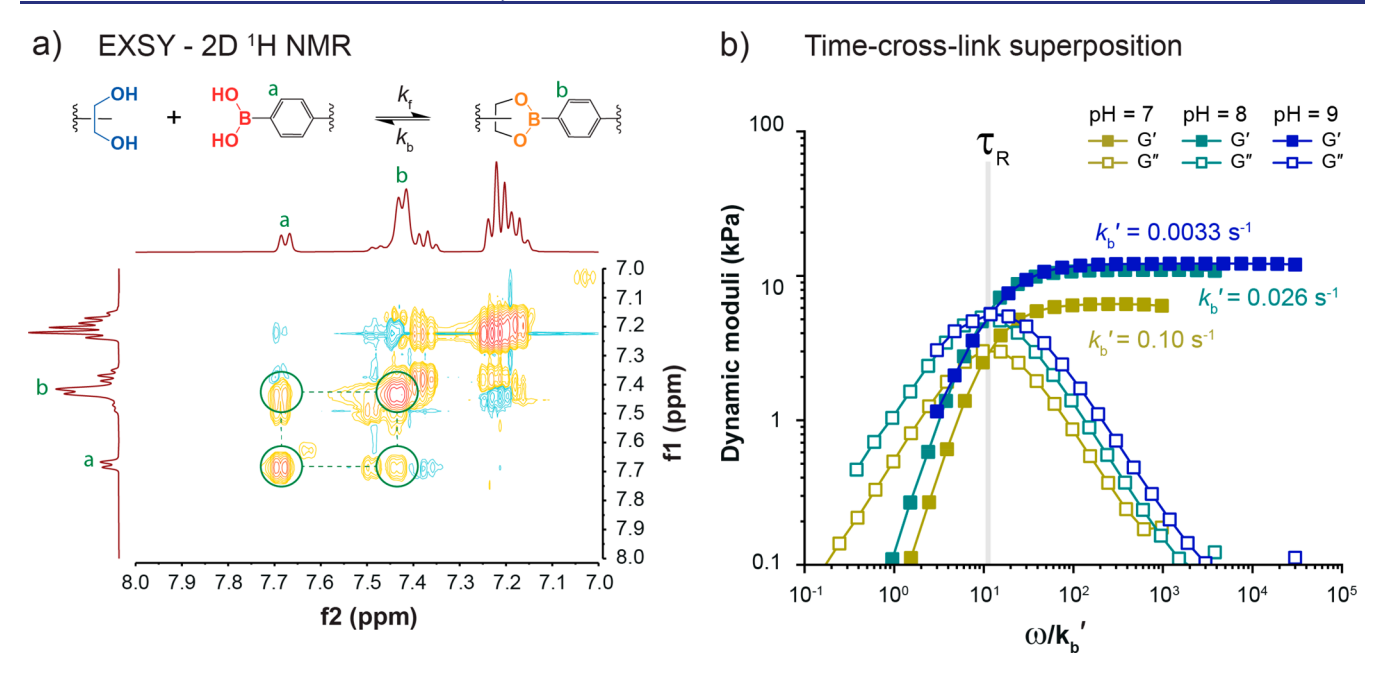


Figure 3. Network rearrangement dynamics in DCvNs scale with the lifetime of the junctions, as measured via exchange NMR spectroscopy (EXSY). (a) Representative 2D  $^{1}$ H NMR spectra for boronic ester formation/dissociation. NOESY experiments were set up to analyze the chemical exchange between phenylboronic acid (PBA) and its corresponding boronic ester. The diagonal and cross-peaks of the bound and unbound aromatic resonances of PBA were integrated to determine the reverse magnetization exchange rate constants,  $k_b$ ′, at different pH. (b) The boronic ester-based hydrogels followed time-cross-link superposition, as the crossover points of the materials between G′ and G″ (a measure of their relaxation time,  $\tau_R$ ) under different conditions (pH = 7, 8, and 9) were scaled by  $k_b$ ′, as determined from EXSY (PEG-PBA/GL, 10 wt %;  $\gamma$  = 1%).

polymer content (Figure 2a). Furthermore,  $G_p$  depends on polymer content, as dictated by classic rubber elasticity, but also on  $K_{\rm eq}$  for boronic ester formation, as expected for a DCvN (Figure 2c).<sup>2</sup> In our work, we further developed a framework to predict  $G_p$  (shear rheometry) based on measurements of  $K_{\rm eq}$  for the boronic ester cross-links (fluorescence-based spectroscopy, <sup>1</sup>H 1D NMR spectroscopy, and DFT calculations) (Table 1). This approach highlights the utility of careful experimental measurements of the small molecule binding pair to describe macroscale behavior in DCvNs. Nevertheless, the larger question remains: how are  $G_p/K_{\rm eq}$  and  $\tau_R/k_{\rm b}$  controlled by the chemical landscape at the dynamic junctions in DCvNs?

Molecular Behavior in DCvNs Define Network Properties Across a Range of pH. The relation between molecular behavior and macroscale properties (Table 1) was determined for one set of thermodynamic conditions (pH 8, 25 °C). To further characterize how the environment controls chemistry and how chemistry in turn governs properties, we investigated a wider range of conditions. pH was controlled in the DCvNs from pH 4 to 14 (SI Section 4).

Extending the pH range revealed that network formation and stability were significantly affected by pH. In fact, gels were not able to form in the PEG-PBA/GL system below pH 6 or at pH 14 (Figure 4a). The canonical paradigm is that boronic ester formation occurs at pH values at or above the  $pK_a$  of the boronic acid. The "charge rule" was proposed to determine the pH-dependent reactivity of boronic esters, which postulates that the "optimal" pH for ester formation (highest  $K_{\rm eq}$ ) lies between the  $pK_a$  values of the boronic acid and the diol:  $pH_{\rm optimal} = (pK_{\rm a,acid} + pK_{\rm a,diol})/2$  (eq 5). This implies that in our system  $(pK_{\rm a,PBA} = 7.9$  and  $pK_{\rm a,GL} \approx 12)$ , on gels should

form below pH  $\approx$  8, and the optimal pH for gel formation should be around 10.

The reality was more subtle. In contrast to the standard model, our work demonstrated that gels formed up to two pH units below the p $K_{\rm a,PBA}$  and that some of these gels were as robust as those formed at pH above the p $K_{\rm a,PBA}$ . Furthermore, a dip in  $G_{\rm p}$  was observed at pH 10: the predicted optimum by the "charge rule" (Figure 4a). Finally, the dynamics of the network evolved dramatically with pH. Under slightly acidic conditions (pH 6), the networks were highly dynamic,  $\tau_{\rm R}\approx 0.1$  s, while under very basic conditions (pH 13), the networks were more static,  $\tau_{\rm R}\approx 1000$  s, an increase of more than 4 orders of magnitude (Figure 4b). These data suggest that the intricate reaction landscape of boronic ester formation results in complex network behavior.

Boronic Ester Reaction Landscape Drives Complex Network Behavior. As it was evident that DCvN properties emerge from the underlying dynamic covalent chemistry at the junctions, we hypothesized that the reaction pathways (thermodynamics and kinetics) involved in boronic ester formation and dissociation would clarify the unexpected network behavior (Figure 4c). Therefore, we analyzed the chemical reactivity of the individual species at different pH. Our goal was to rationalize complex network stability and dynamics from the chemical reactivities and favored reaction pathways under different environmental conditions.

The chemical equilibrium for boronic ester formation is sensitive to pH because the three main species involved (boronic acid, diol, and boronic ester) have unique electronic properties and reactivities depending on their respective protonation states.<sup>34</sup> Therefore, we considered the respective acid—base equilibria of boronic acid, boronic ester, and diols (Scheme 1).

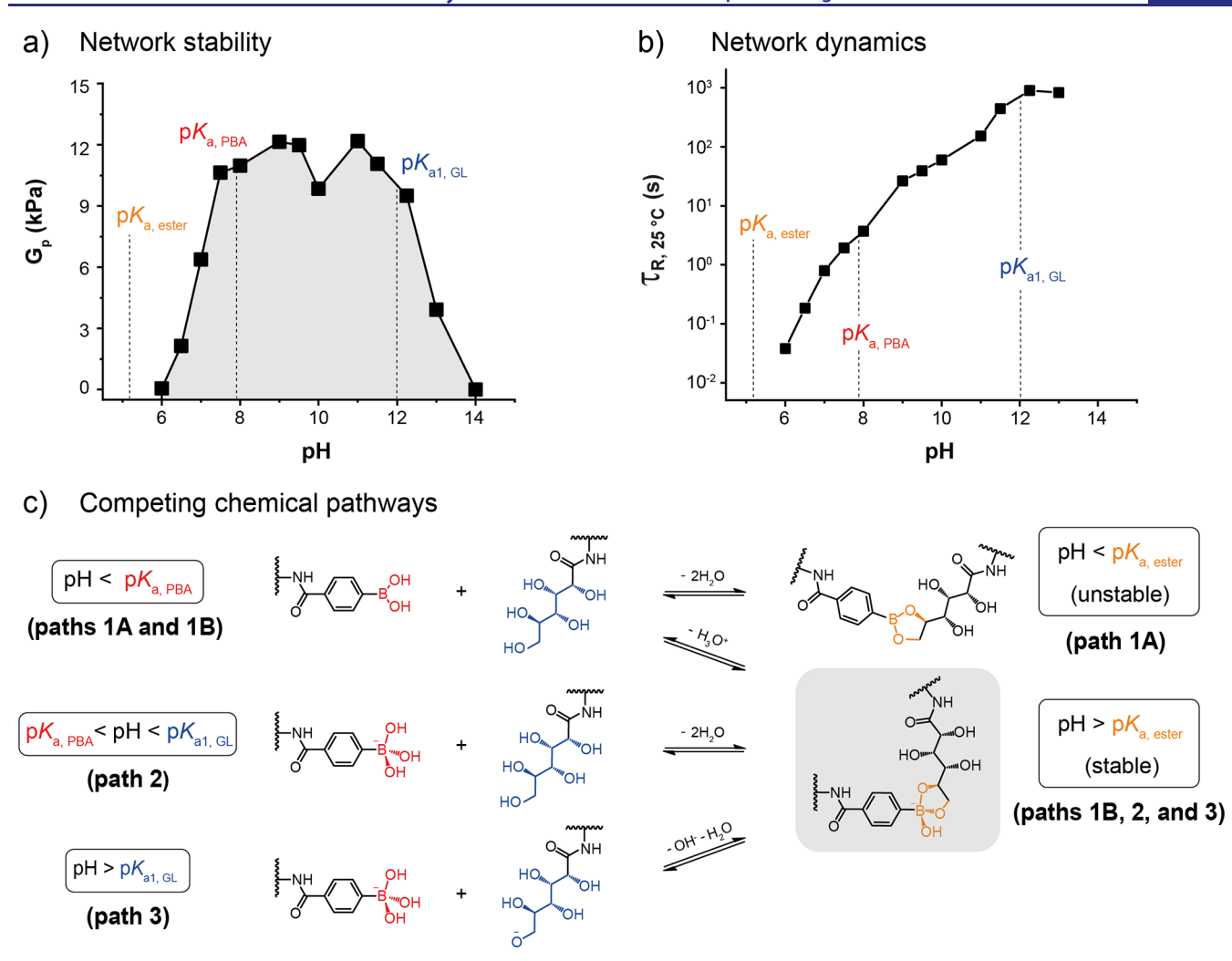


Figure 4. Boronic ester reaction landscape drives complex network behavior in PEG-PBA/GL networks. (a) The network stability, as defined by the plateau modulus,  $G_p$ , and (b) the network dynamics, as defined by the relaxation time,  $τ_R$ , varied strongly with pH (PEG-PBA/GL, 10 wt %; γ = 1%). (c) Depending on the protonation state of the reactants, boronic acids (PEG-PBA; red) and diols (PEG-GL; blue), and of the products, boronic/boronate ester (PEG-PBA/GL; orange), the reaction proceeds along different pathways. At any given pH, the protonation state of the species is determined by their respective  $pK_a$  values:  $pK_{a,PBA} = 7.9$ ,  $pK_{a1, GL} \approx 12$ , and  $pK_{a,ester} = 5.2$ . At low pH, both reactants are fully protonated; the reaction proceeds either through path 1A (when neutral boronic esters are formed) or through path 1B (when anionic boronate esters are formed). At higher pH, the hydroxylation of the boronic acids shifts the reaction to path 2, while at even higher pH, path 3 is preferred, as the diol deprotonates.

Under acidic conditions, boronic acids—weak organic Lewis acids—exist in the neutral form with a trigonal planar (sp²) boron center with O–B–O bond angle of  $\approx 120^{\circ}$  (Scheme 1a). Neutral boronic acids are electrophilic, based on the vacant porbital on the boron, and highly reactive toward nucleophiles, such as diols. Conversely, under basic conditions, the electron-deficient boron is attacked by nucleophilic hydroxide ions, forming a hydroxyboronate anion. Here, the boron hybridizes to sp³, adopting a tetrahedral configuration with O–B–O bond angle of  $\approx 109.5^{\circ}$ . The anionic boronic acid is far less reactive than the neutral form, as the boron no longer possesses a vacant p-orbital.<sup>35</sup>

This explains why the esterification reaction rate constant,  $k_{\rm f}$  is inversely proportional to pH. The preferred kinetic pathway occurs through diol addition to the neutral boronic acid, independent of pH, rather than through substitution of the hydroxyl ion in the anionic species, as was proposed originally.<sup>34</sup> This was supported by our observation that the gelation time,  $t_{\rm gel}$  in boronic ester-based gels increased with

pH (SI Section 7.2), as seen for other boronic ester networks.<sup>36</sup> A direct link between  $t_{\rm gel}$  and  $k_{\rm f}$  has also been observed in other DCvNs.<sup>37,38</sup>

pH-Dependent Stability of Boronic Esters at the Junctions Determines Network Modulus. While the boronic acid reactivity explained how fast the networks formed,  $G_p$  was controlled by the pH-dependent stability of the boronic ester junctions. We reasoned that boronic esters, like boronic acids, exist in acid—base equilibrium between neutral (sp²) and anionic (sp³) forms (Scheme 1b). When a boronic acid binds to a diol to form a cyclic boronic ester, the Lewis acidity of the boron increases, as the driving force for rehybridization from sp² to sp³ is increased by the associated release of ring strain going from 120° to 109.5°. Thus, the p $K_a$  of the boronic ester is always lower than that of the corresponding boronic acid. For example, the p $K_a$  of phenylboronic acid decreases from 8.8 to 6.8 upon esterification with glucose. 90 Our DFT calculations showed

# Scheme 1. Acid—Base Equilibria of the Main Species Involved in Boronic Ester Complexation<sup>a</sup>

# a) boronic acid

$$R_1-B$$
 +  $2H_2O$   $R_1-B$  OH +  $H_3O$ 

# b) boronic ester

$$R_1 - B \longrightarrow R_3$$
 +  $2H_2O \longrightarrow R_1 - B \longrightarrow R_3$  +  $H_3O$ 

$$HO$$
  $R_2$   $+$   $H_2O$   $K_{a1, GL}$   $HO$   $R_2$   $+$   $H_3O$   $R_3$ 

<sup>a</sup>For a given pH, the relative abundance of the neutral and anionic forms of all the species can be determined from their  $pK_a$  (the pH at which 50% of the neutral groups are converted to their anionic forms). For example, at pH =  $pK_a \pm 1$ , 10%/90% of the neutral species are present.

that the p $K_a$  of the ester decreases from 7.9 to 5.2 for PEG-PBA/GL (SI Section 5.2), in agreement with the literature.<sup>40</sup>

In this way, the Lewis acidity of the boronic esters explained network formation in the PEG-PBA/GL system. We observed nascent gel formation at pH 6, when ≈90% of the cross-links were anionic esters (p $K_{a,ester} = 5.2$ ), and robust gel formation starting at pH 7, when ≈99% of the cross-links were anionic esters (Figure 4a). Therefore, we hypothesized that the reaction proceeded via path 1A or path 1B, until pH 10 (Figure 4c). In both paths, the neutral boronic acid and the fully protonated diol are the reactive species, but the product is either a neutral boronic ester (path 1A) or an anionic boronate ester (path 1B), depending on the pH (detailed mechanism in Figure 5). At pH < p $K_{a,ester}$ , path 1A dominated, and neutral boronic esters were favored, which are highly reactive (empty p-orbital) and prone to hydrolysis (high angle strain). As a result, at pH < 6, gelation was not observed (Figure 4a). Conversely, at pH >  $pK_{a,ester}$ , path 1B dominated. Here, anionic boronate esters were favored, which formed stable cross-links, corresponding to robust network formation with high  $G_p$  (Figure 4a).

Interestingly, gel formation was observed beyond pH 10, at which point there should be very few neutral boronic acids  $(sp^2)$  left to react  $(pK_{a,PBA} = 7.9)$ . This implies a change in the mechanism from **path 1B** to **path 2**, wherein the anionic boronate  $(sp^3)$  becomes the reactive species, though at a slower rate. This rationalized the dip in  $G_p$  at pH 10, as in **path 2** both of the reactants—the fully protonated diol and the anionic boronate—are relatively stable and unreactive.

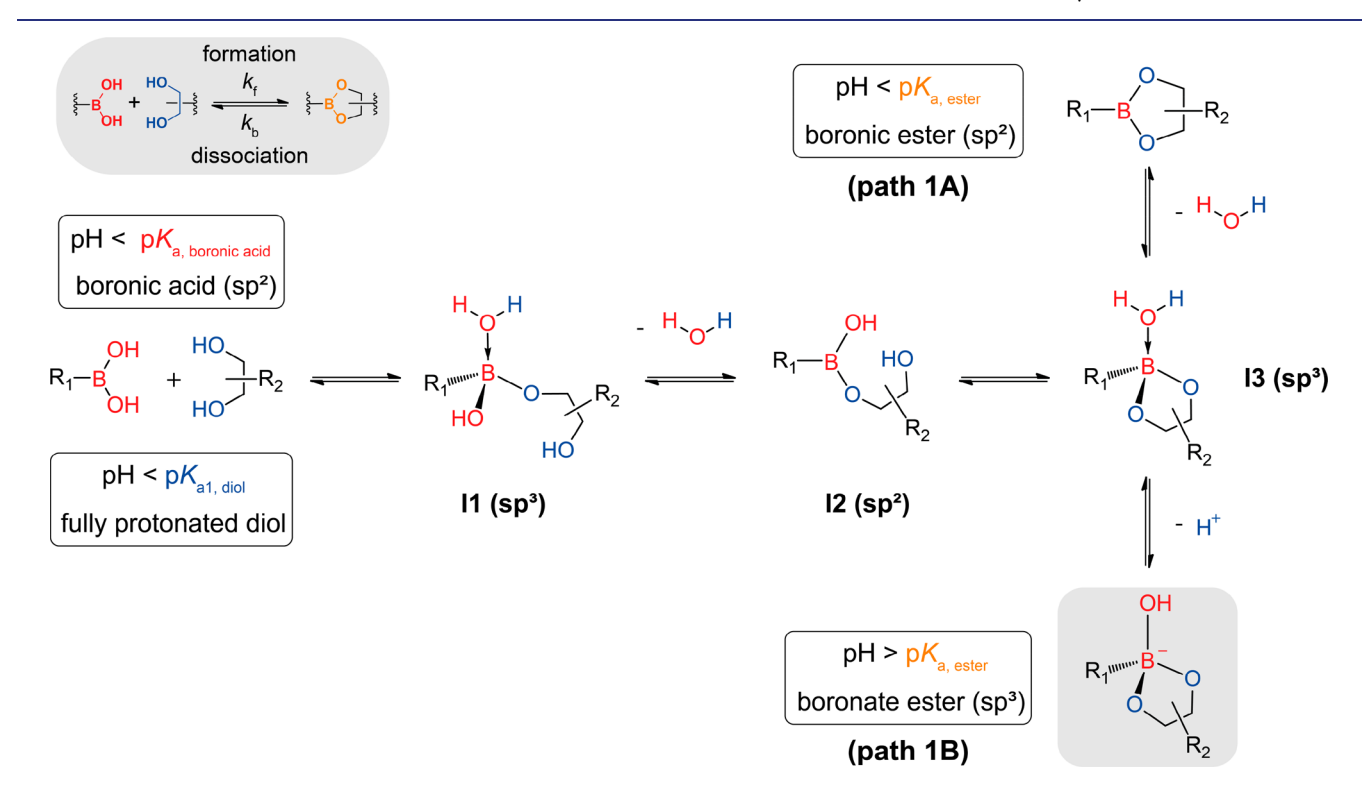
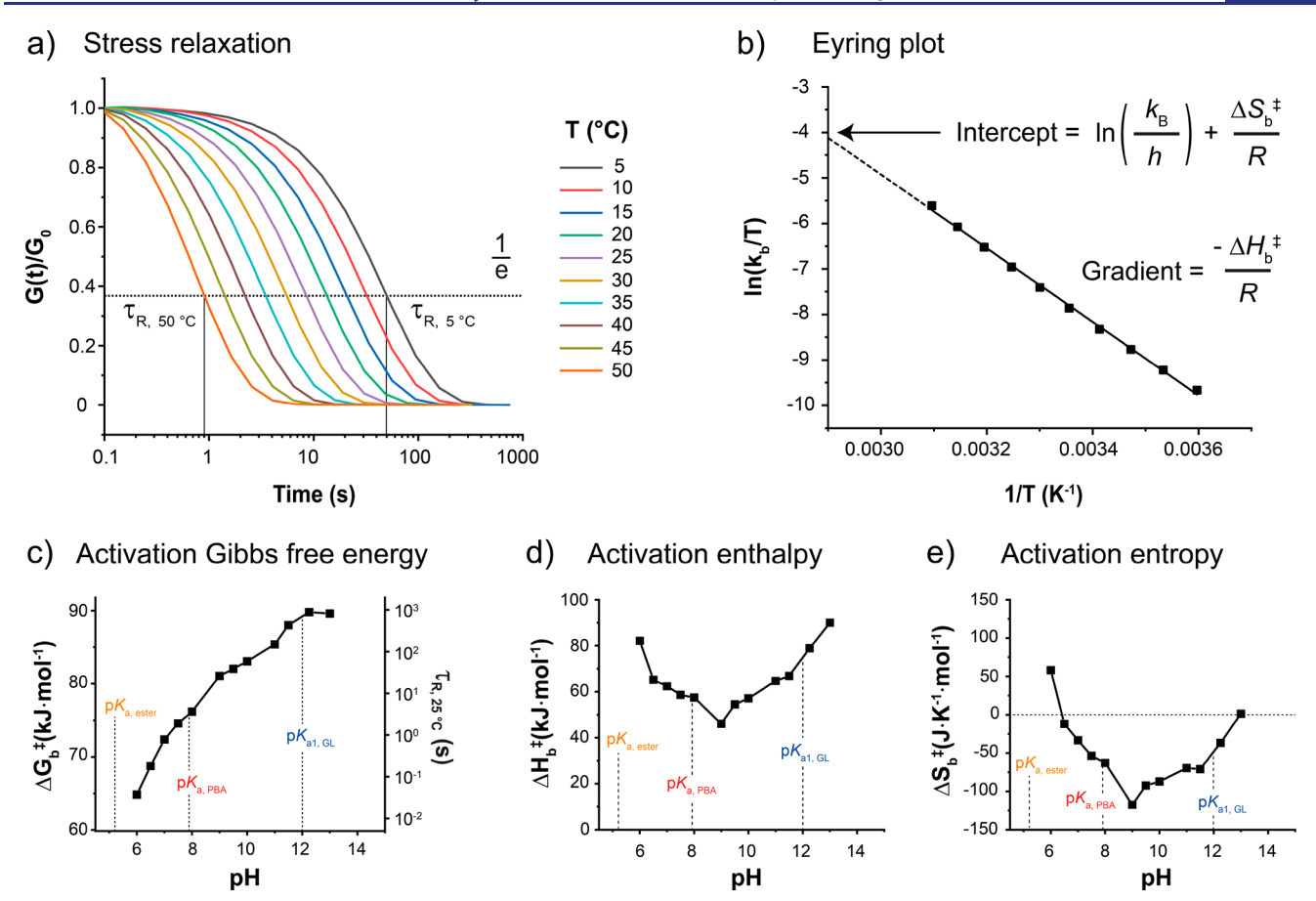


Figure 5. Proposed reaction mechanism for boronic and boronate ester formation/dissociation at pH < 10. For dissociation under basic conditions (path 1B), the anionic boronate ester (sp<sup>3</sup>) first protonates to form a neutral intermediate with a water molecule coordinated to the tetrahedral boron (I3; sp<sup>3</sup>). In the next step, the ester ring opens to form a reactive trigonal planar intermediate (I2; sp<sup>2</sup>). Water once again coordinates to boron to form another tetrahedral intermediate (I1; sp<sup>3</sup>). In the final step, the boronate ester bond fully dissociates into a neutral boronic acid (sp<sup>2</sup>) and a fully protonated diol. For dissociation under acidic conditions (path 1A), the starting species is the neutral boronic ester (sp<sup>2</sup>), which directly coordinates to water to form I3. Subsequent steps are the same as in path 1B. In both cases, sp<sup>2</sup> and sp<sup>3</sup> hybridized intermediates are necessary for the ester dissociation.



**Figure 6.** Transition State Theory and rheology quantitatively describe the reaction landscape at the cross-links in ideal DCvNs. (a) Stress relaxation experiments showed an Arrhenius-type temperature dependence of the relaxation time,  $\tau_{\rm R}$ , (PEG-PBA/GL, pH 8, 10 wt %;  $\gamma = 10\%$ ). (b) The Eyring equation was used to calculate the temperature dependence of the backward reaction rate,  $k_{\rm b}$ , by assuming that  $k_{\rm b} = 1/\tau_{\rm R}$  (PEG-PBA/GL, pH 8, 10 wt %;  $\gamma = 10\%$ ). (e) The backward activation Gibbs free energy,  $\Delta G_{\rm b}^{\dagger}$ , was calculated using eq 6 from (d) the backward activation enthalpy,  $\Delta H_{\rm b}^{\dagger}$ , and (e) the backward activation entropy,  $\Delta S_{\rm b}^{\dagger}$ , which were both obtained from the Eyring plots at different pH.

However, the decrease in  $G_{\rm p}$  was confined to a small pH window, as the thermodynamic landscape changes again at even higher pH. The hydroxyl groups in GL begin to deprotonate (p $K_{\rm a,GL}\approx 12$ , Scheme 1c), and the deprotonated diols are highly reactive toward boron, including the anionic boronate, because the oxyanion is a stronger nucleophile than the hydroxyl anion (path 3).

It is only in strongly basic environments (pH > 12), that  $G_p$  decreased significantly, and networks did not form at pH 14 (Figure 4a). Hydrolysis of the PEG backbone was initially hypothesized to account for the inability to form gels at pH 14, but this was discarded as we observed that gel precursor solutions prepared at pH 14 subsequently formed a gel when their pH was adjusted to a lower value. Possible alternative explanations include charge—charge repulsion between the anionic boronate and a twice deprotonated GL, or hydrolysis of the boronate ester itself by hydroxyl anions.

Boronic Ester Dissociation Governs Network Dynamics. Above, we established that the complex reaction landscape of boronic ester formation governs the macroscopic stability and modulus of our DCvNs. We then hypothesized that the chemical landscape of boronic ester dissociation (Figure 5) would explain the dynamics and adaptability of boronic esterbased DCvNs, as  $\tau_R$  is inversely related to the kinetics of bond dissociation,  $k_b$  (eq 4). Since the anionic boronate ester was

presumed to be the principal network forming species, our analysis focused on the backward reaction of path 1B.

When a boronate ester dissociates into boronic acid and diol, several intermediates are formed. While the precise mechanism is still debated, it is generally accepted that both sp<sup>2</sup>- and sp<sup>3</sup>-hybridized intermediates are present.<sup>41</sup> In our proposed reaction mechanism shown in Figure 5, the anionic boronate ester (sp<sup>3</sup>) first protonates to form a neutral intermediate (I3), with a water molecule coordinated to the tetrahedral boron, with sp<sup>3</sup>-hybridization. In the next step, the ester ring opens to form a very reactive trigonal planar intermediate (I2). Here, the hybridization state of the boron center changes from sp<sup>3</sup> to sp<sup>2</sup>. Again, water coordinates with boron to form another tetrahedral intermediate (I1), and the hybridization state reverts to sp<sup>3</sup>. In the final step, the boronate ester bond fully dissociates into a neutral boronic acid (sp<sup>2</sup>) and a fully protonated diol.

The kinetics of the boronate ester dissociation in our proposed reaction depend on the relative energies of the various intermediates (and their associated transition states). This energetic landscape is highly sensitive to pH, as the relative energies of the sp²- and sp³-hybridized boron species depend on pH (Scheme 1). Under basic conditions, the sp³-hybridized species (I1 and I3) are lower in energy, while acidic conditions favor the sp²-hybridized species (I2). This implied that the dissociation dynamics should be fastest at the pH

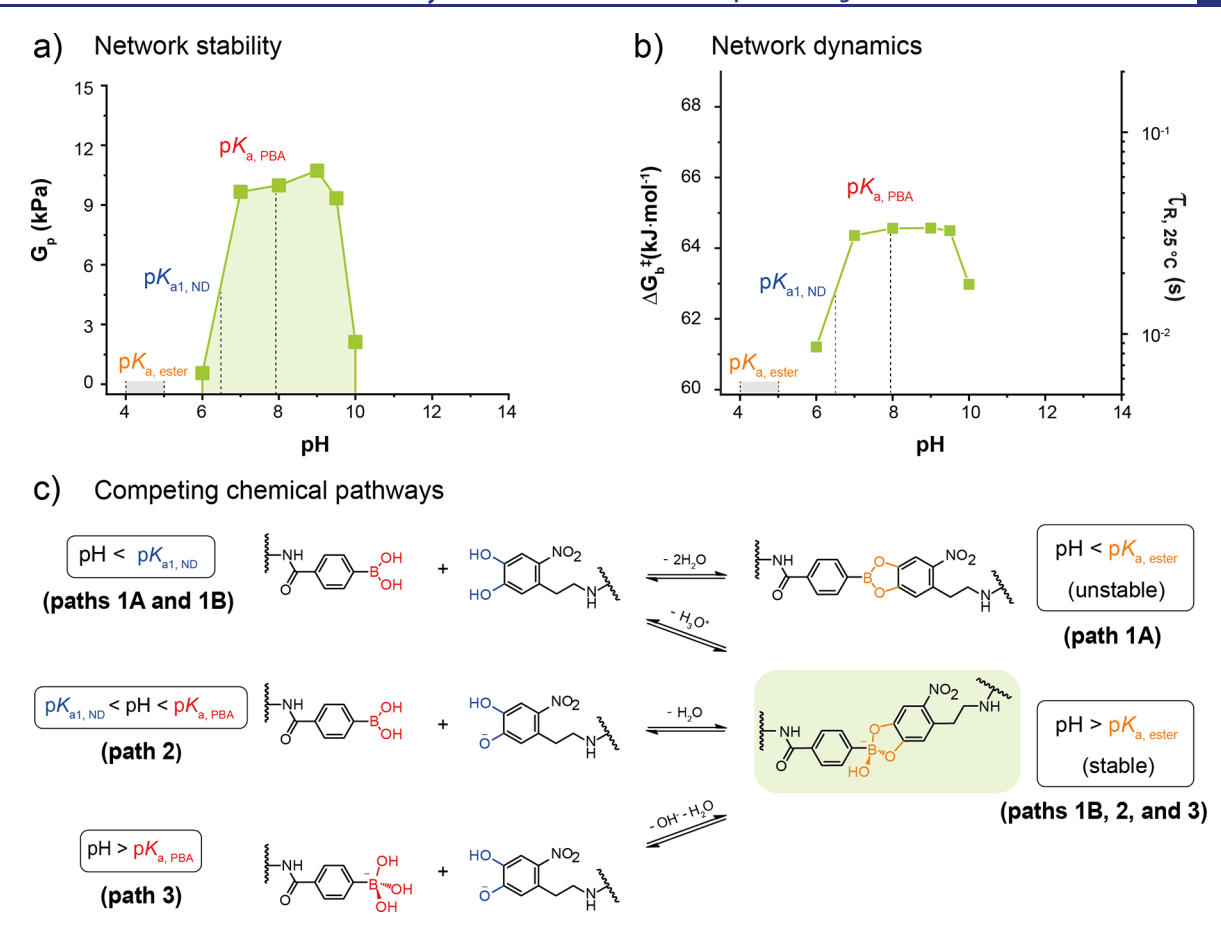


Figure 7. Distinct macroscopic behavior arises from contrasting molecular behavior at the junction of PEG-PBA/ND networks. (a) Stable gels formed from pH 6 to 10. Within this narrow range, both the plateau modulus,  $G_p$ , and (b) the relaxation time,  $\tau_R$ , remained stable (PEG-PBA/ND, 10 wt %;  $\gamma = 1\%$ ). (c) The boronic ester reaction landscape drives the complex pH-dependent network behavior. The reaction proceeds along different pathways depending on the protonation state of the reactants, boronic acids (PEG-PBA; red) and diols (PEG-ND; blue), and of the products, boronic/boronate ester (PEG-PBA/ND; orange). Their protonation state at a given pH is determined by their respective  $pK_a$  values:  $pK_{a, PBA} = 7.9$ ,  $pK_{a1, ND} \approx 6.5$ , and  $pK_{a, ester} \approx 4-5$ . At low pH, both reactants are fully protonated; the reaction proceeds either through **path 1A** (when neutral boronic esters are formed) or through **path 1B** (when anionic boronate esters are formed). Unlike the PEG-PBA/GL system, hydroxylation of the boronic acid occurs at a higher pH than diol deprotonation. Thus, differences in **paths 2** and 3 for the two types of networks can account for their diverging behavior at higher pH and the inability of the PEG-PBA/ND network to form above pH 10.

where both  $\rm sp^2$  and  $\rm sp^3$  species are energetically accessible, since both are involved in the dissociation reaction. While in practice the  $\rm pK_a$  of the intermediates are challenging to determine, they are expected to be similar to  $\rm pK_{a,ester}$  and  $\rm pK_{a,PBA}$ . Therefore, as pH increases above  $\rm pK_{a,ester}/\rm pK_{a,PBA}$ , the energy difference between the  $\rm sp^2$  and  $\rm sp^3$  intermediates increases, leading to slower reaction kinetics. This trend was reflected in the network dynamics of the gels, which slowed considerably with increasing pH (Figure 4b).

This reaction inspection demonstrates how complex network behavior in DCvNs arises from nuanced molecular behavior at the dynamic junction. As the reaction landscape is highly dependent on environmental conditions (pH), it is critical to consider preferential reaction pathways at different conditions to understand macroscale behavior in DCvNs. Further, the chemical landscape at the dynamic junction can explain noncanonical behavior. For example, in the boronic ester-based networks, an unexpected dip in  $G_{\rm p}$  was observed at pH 10, the "optimal" pH for network formation based on the "charge rule". We rationalized this effect by realizing that the preferred reaction pathway changes near this pH, highlighting potential limitations of simplified chemical explanations for complex networks.

Kinetic Studies Directly Within Formed Networks Yield Quantitative Activation Energies. Chemical kinetic studies are a powerful experimental tool to study reaction mechanisms. Transition State Theory and the Eyring equation provide a direct relationship between reaction rate constants and activation energies. However, rate constants can be difficult to determine directly, especially within polymer networks. Having established a robust relation between macroscale network properties and the chemical landscape at the molecular level in DCvNs, we used shear rheometry within our ideal DCvNs to measure activation energies of the dynamic covalent chemistry at the junctions (SI Section 5.6).

Stress relaxation experiments ( $T=5-50~^{\circ}\mathrm{C}$ ) showed a strong temperature dependence for  $\tau_{\mathrm{R}}$  in the boronic esterbased networks (Figure 6a). We constructed Eyring plots from  $\tau_{\mathrm{R}}$  measurements by plotting  $\ln(k_{\mathrm{b}}/T)$  against 1/T (Figure 6b). We assumed that  $k_{\mathrm{b}}=1/\tau_{\mathrm{R}}$ , setting the constant of proportionality in eq 4 to unity (SI Section 7.3). This assumption is reasonable given that  $\tau_{\mathrm{R}}$  has been related directly to  $k_{\mathrm{b}}$  in other DCvNs and in boronic ester-based networks themselves (Figure 3).  $^{14,17,32,38}$  The backward activation enthalpy,  $\Delta H_{\mathrm{b}}^{\,\pm}$ , and entropy,  $\Delta S_{\mathrm{b}}^{\,\pm}$ , were obtained from the slope and the intercept of the Eyring plots, respectively (Figure

6b). The backward activation Gibbs free energy,  $\Delta G_b^{\dagger}$ , was subsequently calculated according to eq 6.

$$\Delta G_{\mathbf{b}}^{\ddagger} = \Delta H_{\mathbf{b}}^{\ddagger} - T \Delta S_{\mathbf{b}}^{\ddagger} \tag{6}$$

Analysis of network dynamics through the lens of Transition State Theory provided insights into the molecular behavior of the boronic ester junctions.  $\Delta G_{\rm b}^{\,\ddagger}$  predicted the macroscopic dynamics of the network; the pH-dependent increase in  $\Delta G_{\rm b}^{\,\ddagger}$  mirrored the increase of  $\tau_{\rm R}$  with pH, from  $10^{-2}$  s to  $10^3$  s (Figure 4b). Here,  $\Delta G_{\rm b}^{\,\ddagger}$  ranged from 65 to 90 kJ mol $^{-1}$ , which was consistent with previous literature reports for boronic esters (Figure 6c).  $^{43,44}$ 

Additional information on the reaction mechanism was provided by  $\Delta H_{\rm b}^{\ddagger}$ ; lower values implied a transition state associated with lower energy bond breaking. In the PEG-PBA/GL system,  $\Delta H_{\rm b}^{\ddagger}$  was high at both ends of the pH spectrum (82 and 90 kJ mol<sup>-1</sup> at pH 6 and 13, respectively), with a minimum around pH 9 (46 kJ mol<sup>-1</sup>) (Figure 6d). We rationalized these enthalpy values by considering that that the reaction pathways require more energy when water coordination and decoordination to boron becomes unfavorable. This occurred, at low and high pH, as the energy of the reaction intermediates increased as pH deviated from p $K_{\rm a,PBA}/pK_{\rm a,ester}$ . Alternatively, the  $\Delta H_{\rm b}^{\ddagger}$  trend could indicate a change in the preferred reaction pathway from path 1B to path 2 near pH 9 (Figure 4c).

 $\Delta S_b^{\ddagger}$  provides insight into the degree of order in the transition state.  $\Delta S_b^{\ddagger}$  was negative across much of the pH range investigated, reaching a minimum at pH 9 (-117 J K<sup>-1</sup> mol<sup>-1</sup>; Figure 6e), implying an associative mechanism with an ordered transition state. This was consistent with findings that boronic ester formation and dissociation are associated with large negative values of  $\Delta S_b^{\ddagger}$ , which indicate an increase in the coordination number of the central boron. Further, the observed  $\Delta S_b^{\ddagger}$  values supported the proposed mechanism in Figure 5, where boron repeatedly changes its coordination number as it undergoes transformations from trigonal (sp<sup>2</sup>) to tetrahedral (sp<sup>3</sup>) geometries.

Thus, Transition State Theory was successfully applied to describe DCvN dynamics. Quantitative activation energies were obtained directly from viscoelastic measurements, providing mechanistic insight into the molecular behavior of the cross-links. In this manner, a shear rheometer can be used as a spectroscopic tool to analyze the physicochemical properties of the dynamic bond in ideal DCvNs. Rheometric measurements are ubiquitous in the understanding of network behavior, and the ability to extend broadly accessible and rapid analysis to inspect reaction landscapes at the junction of DCvNs provides a powerful tool in understanding and exploiting dynamic covalent chemistry in materials design.

Changing Boronic Ester Chemistry at the Junctions Dramatically Alters Macroscopic Network Behavior. Up to here, the discussion was restricted to the PEG-PBA/GL system. The structure and properties of GL resemble those of simple sugars with multiple dangling hydroxyl groups and a high  $pK_a \approx 12$ . There are, however, many other types of diols, such as catechol derivatives, that have very different chemical properties, characterized by rigid coplanar vicinal *cis*-diols and high acidities.

To investigate a broader range of electronic and steric properties in the diol, we exchanged GL for nitrodopamine (ND; Figure 7). The PBA was not changed. ND is a catechol derivative with an electron withdrawing nitro group to mitigate

oxidation.<sup>28</sup> The nitro group lowers the  $pK_a$  of the dopamine from 9 to 6.5. Therefore, in the PEG-PBA/ND system, the  $pK_a$  sequence was different ( $pK_{a,ester} < pK_{a1,ND} < pK_{a,PBA}$ ) than that in the PEG-PBA/GL system ( $pK_{a,ester} < pK_{a,PBA} < pK_{a1,GL}$ ). At low pH, the behaviors of both PEG-PBA/GL and PEG-PBA/ND systems exhibited similarities. Network formation was first observed at pH 6, with similar  $G_p$  values (Figures 4a, 7a). In both systems, gelation required formation of the anionic boronate ester. This occurred at pH >  $pK_{a,ester}$  through paths 1B, 2, or 3 (Figures 4c, 7c).

However, the preferred reaction pathway in the two systems is different, because ND is more acidic than PBA (pK<sub>a1,ND</sub><  $pK_{a,PBA}$ ) and GL is more basic than PBA ( $pK_{a,PBA} < pK_{al,GL}$ ). Consequently, path 1B is preferred for PEG-PBA/GL. This is because in path 2, the reactants—anionic boronate acid and fully protonated diol—are both stable and unreactive species (Figure 4c). On the other hand, in PEG-PBA/ND, path 2 dominates, as the reaction between the monodeprotonated diol (a nucleophilic oxyanion) and the neutral boronic acid (with its empty p-orbital) is favored (Figure 7c). At higher pH, additional differences appear. In contrast to PEG-PBA/GL, PEG-PBA/ND was unstable in basic conditions; network formation was not observed above pH 10 (Figure 7a). We hypothesized that network formation in PEG-PBA/ND was inhibited at high pH via charge-charge repulsion; the anionic boronate acid is unable to bind the monodeprotonated diol (path 3) or the doubly deprotonated diol (since  $pK_{a2,ND} \approx$ 

Strikingly, the kinetics in PEG-PBA/ND were significantly faster than those in PEG-PBA/GL. The most dynamic PEG-PBA/GL network (pH 6) had a similar  $\tau_{\rm R}$  (0.04 s) as the least dynamic PEG-PBA/ND network (pH 9;  $\tau_{\rm R}$  = 0.035 s). For comparison,  $\tau_{\rm R}$  for PEG-PBA/GL at pH 9 was 25 s (Figures 4b and 7b). Thus, networks containing ND were orders of magnitude more dynamic than networks containing GL at the same pH, yet with similar  $G_{\rm p}$ .

Quantifying  $K_{\rm eq}$  Highlights Molecular Differences in Network Behavior. In DCvNs,  $\tau_{\rm R}$  and  $G_{\rm p}$  change with temperature, as they are related to  $k_{\rm b}$  and  $K_{\rm eq}$  respectively, which are both temperature-dependent:  $k_{\rm b}$  through the Eyring equation and  $K_{\rm eq}$  according to eq 3 (assuming a constant  $\Delta_{\rm r}G^{\circ}$ ). Therefore, the thermodynamics of the cross-links were related to  $G_{\rm p}$  through precise rheometric measurements of PEG-PBA/GL and PEG-PBA/ND, just as  $\tau_{\rm R}$  provided insight into the kinetics of cross-link formation and dissociation.

Measurements of G<sub>p</sub> from 5 to 50 °C in PEG-PBA/GL revealed contrasting behaviors at different pH. At low pH (6 and 7),  $G_p$  decreased as a function of T (Figure 8a). At higher pH, the trend was reversed: G<sub>p</sub> was stable (pH 8) or even increased with T (pH 9). These contradictions resulted from the competing factors that determine  $G_p$  in DCvNs. Classic thermoelastic effects arise from the entropic penalty for deforming network strands, causing  $G_p$  to increase directly with T (eq 1). However, in our DCvNs, the number density of elastically active network strands is related to  $K_{\rm eq}$  through p (eq 2). Therefore, the thermoelastic effect can be counterbalanced by a decrease in the number density of elastically active network strands by changes in  $K_{\rm eq}$ . When  $K_{\rm eq} \to \infty$ , as in permanent covalent networks,  $p \to 1$  and the dynamic phantom network model converges to the standard phantom network model (thermoelasticity). This was the case for PEG-PBA/GL at pH 9, where  $G_p$  increased linearly with T. At pH 7,  $G_p$  decreased with T. This inverse thermoelastic behavior

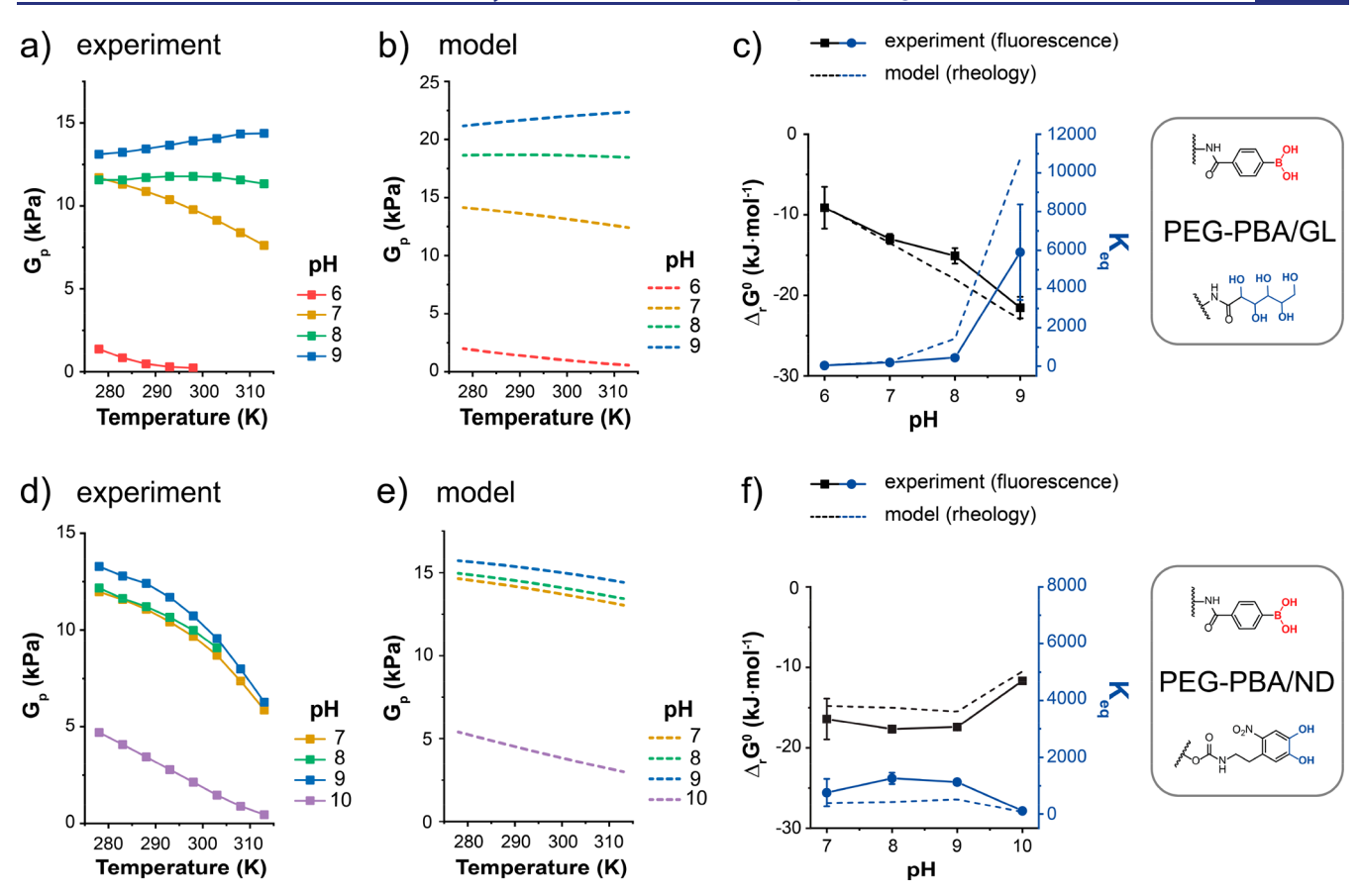


Figure 8. Thermodynamics at the junctions of DCvNs probed by rheological measurements as a function of temperature. The plateau modulus,  $G_{\rm p}$ , was measured at different temperatures and pH in the (a) PEG-PBA/GL and (d) PEG-PBA/ND systems (10 wt %;  $\gamma=1$ %). (b,e) The rheological data were fitted to the dynamic model, yielding at each pH the reaction Gibbs free energy,  $\Delta_{\rm r}G^{\circ}$ . Subsequently, the equilibrium constant,  $K_{\rm eq}$  was calculated using eq 3. (c,f)  $\Delta_{\rm r}G^{\circ}$  and  $K_{\rm eq}$ , obtained from the rheological model, were compared to  $K_{\rm eq}$  determined at the same pH from the fluorescence-based competitive displacement assay (25 °C).

occurred because  $K_{\rm eq} \to 1$  and  $p \to 0$ , as T increased. At pH 8, the opposing forces that govern  $G_{\rm p}$ , entropic elasticity and  $K_{\rm eq}$ , compensated each other and  $G_{\rm p}$  was independent of T (Figure 8a).

Our rheometric analyses were also used to quantify  $K_{\rm eq}$  at different pH. The  $G_{\rm p}$  data were fitted to the dynamic phantom network model (Figure 8b). For each pH, a single value for  $\Delta_{\rm r}G^{\circ}$  was calculated, which was used to determine  $K_{\rm eq}$  at each T (eq 3). For the fitting, both the general trend—whether  $G_{\rm p}$  increased, was stable, or decreased with T—and the magnitude of  $G_{\rm p}$  were considered. The results were in good agreement with fluorescence-based measurements of  $K_{\rm eq}$  (Figure 8c), further demonstrating how the rheometer can be used as a molecular spectroscopic tool.

In addition, this approach highlighted molecular-scale differences between PEG-PBA/GL and PEG-PBA/ND, which were not apparent initially from macroscopic studies as  $G_{\rm p}\approx 10$  kPa for both systems (pH 7–9; 25 °C). However, distinct behaviors emerged in the two networks for the relationship between  $G_{\rm p}$  and T.

The interesting behavior for  $G_{\rm p}$  as a function of T in the PEG-PBA/GL system indicated large  $K_{\rm eq}$  variations over a narrow pH window. According to the spectroscopic measurements,  $K_{\rm eq}$  increased from 40  $\pm$  26 at pH 6 to 5906  $\pm$  2470 at pH 9. The rheometric data exhibited a similar increase in  $K_{\rm eq}$  from 37 at pH 6 to 10750 at pH 9 (Figure 8c). For PEG-PBA/ND,  $G_{\rm p}$  decreased with T across all pH tested, indicating that

 $K_{\rm eq}$  was comparatively lower and more constant. These findings were confirmed quantitatively by shear rheometry and the fluorescence-based spectroscopy, both of which showed that  $K_{\rm eq}$  remained relatively unchanged from pH 7 and 9. At pH 9,  $K_{\rm eq}$  = 1126  $\pm$  108 and 520 (from spectroscopy and rheology, respectively) and then decreased sharply at pH 10 to  $K_{\rm eq}$  = 112 and 70 (Figure 8e,f). The measured values for  $K_{\rm eq}$  between PEG-PBA and PEG-ND were surprising, as literature reports have shown that  $K_{\rm eq}$  for small molecule catechol—boronic acid pairs are 2 orders of magnitude larger than the complexes formed by conformationally more flexible saccharides. In fact, the presence of the nitro group, which significantly lowers the  $pK_{\rm a}$  of the diol, could explain some of the differences in  $K_{\rm con}$ 

the differences in  $K_{\rm eq}$ . Elucidating B–N Interactions in Wulff-Type Boronic Acids Using Rheology. Boronic acids are implemented industrially as receptors for the selective separation and molecular recognition of *cis*-diol containing compounds. Wulff-type *ortho*-aminomethylphenylboronic acids (APBA) enable diol binding in the desired pH range of most biosensors (pH 4.5–8.0), as the aminomethyl group in the ortho position lowers the pKa. Understanding and quantifying the binding interaction of different boronic acid and diol pairs is essential for high affinity and selectivity. However, this remains a challenge as it is difficult to distinguish preferred kinetic paths (due to the effects of "proton ambiguity") and because of the strong medium dependence of these systems.

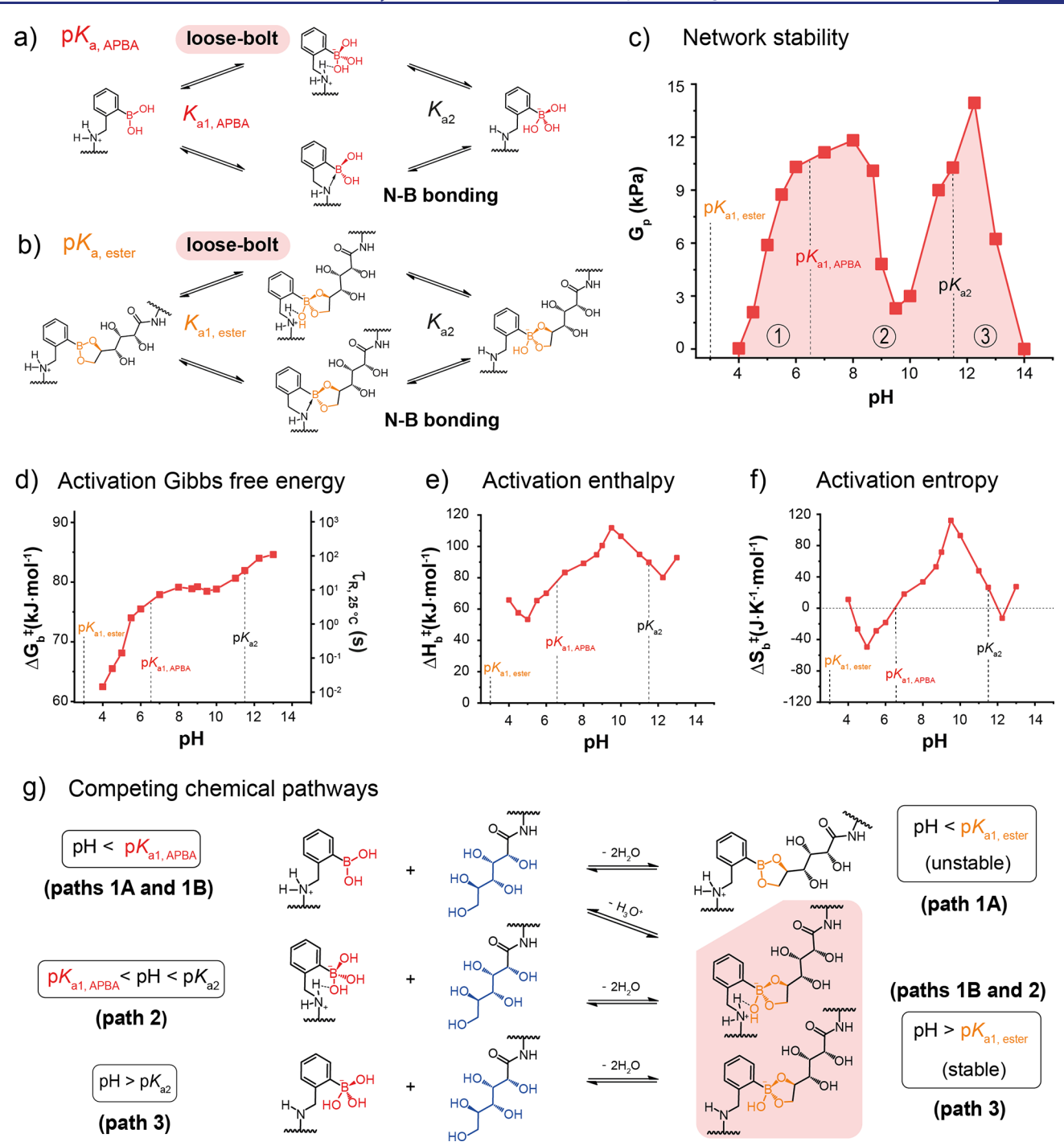


**Figure 9.** Rheometric analysis of the PEG-APBA/GL system corroborates the "loose-bolt" postulate for Wulff-type boronic acids. The acid—base equilibria for (a) the Wulff-type boronic acid PEG-APBA and (b) its corresponding boronic ester PEG-APBA/GL are characterized by two  $pK_a$  values. In the "N−B bonding" postulate,  $pK_{a1}$  corresponds to the deprotonation of the nitrogen, while  $pK_{a2}$  corresponds to the hydroxylation of the boron. In the "loose-bolt" postulate,  $pK_{a1}$ , APBA/ester corresponds to hydroxylation of the boronic acid/ester and  $pK_{a2}$  corresponds to the deprotonation of the nitrogen. (c) The plateau modulus,  $G_p$ , of the gels varied as a function of pH with two maxima (PEG-APBA/GL, 10 wt %;  $\gamma = 1\%$ ). (d) The backward activation Gibbs free energy,  $\Delta G_b^{\dagger}$ , was calculated using eq 6 from (e) the backward activation enthalpy,  $\Delta H_b^{\dagger}$ , and (f) the backward activation entropy,  $\Delta S_b^{\dagger}$ , which were both obtained at different pH from the Eyring plots of the network relaxation time,  $\tau_R$ . (g) Distinct ranges of pH corresponded to specific reaction pathways. (1) At low pH ( $pK_{a1}$ , ester = 3.0 < pH <  $pK_{a1}$ , APBA = 6.5), PEG-APBA/GL networks formed via **path 1B**. (2) At intermediate pH ( $pK_{a1}$ , APBA = 6.5 < pH <  $pK_{a2} \approx 11$ ), the reaction mechanism shifted to **path 2**. (3) At high pH ( $pK_{a2} \approx 11$  < pH), a new APBA/GL ester species was formed and network formation followed **path 3**.

Despite the broad utility of APBA, the nature of the molecular interaction between the boron and nitrogen in the proximal amine remains unclear. Initially, it was postulated that a dative bond forms between N and B with near sp<sup>3</sup> hybridization, stabilizing APBA at neutral pH ("N–B bonding"

postulate; Figure 9a,b).<sup>51</sup> Recently, Anslyn and co-workers have pointed to <sup>11</sup>B NMR and computational studies as evidence that a solvent-inserted species is dominant in protic media for both boronic acids and boronate esters ("loose-bolt" postulate; Figure 9a,b).<sup>22</sup> In both cases,  $pK_a$  values can be

assigned to the boron and nitrogen centers, although their order depends on the postulate. In the "N–B bonding" postulate,  $pK_{a1}$  corresponds to the deprotonation of the nitrogen (pH 6–7), while  $pK_{a2}$  corresponds to the hydroxylation of the boron and breaking of the N–B bond, which is in the range of most boronic acids (pH 9–10). Conversely, in the "loose-bolt" postulate,  $pK_{a1}$  corresponds to hydroxylation of the boronic acid/ester (pH 5–7), which gives a solvent-inserted structure.  $pK_{a2}$  then corresponds to the deprotonation of the nitrogen (pH 10–12), (Figure 9a,b).<sup>22</sup>

Rheology of PEG-APBA-GL Corroborates the "Loose-Bolt" Postulate. Having demonstrated the ability to elucidate molecular interactions directly from rheometric measurements, we applied our approach to clarify the reaction mechanism of Wulff-type boronic acids. We synthesized PEG-APBA/GL networks across a wide range of pH (pH 4-14). G<sub>p</sub> varied as a function of pH with two maxima, suggesting a pH-dependent transition in reaction pathways (Figure 9c). Potentiometric studies on APBA moieties by Bosch et al. demonstrated pHdependent formation of two species: a zwitterionic species with maximal concentration at pH 6 and an anionic species at pH 11. $^{34,40}$  Therefore, we hypothesized that the peak in  $G_p$  at pH 8 was due to the presence of a zwitterionic ester (the APBA/GL ester from paths 1B and 2) and that the peak at pH 12.5 was due to an anionic ester (the fully deprotonated product from path 3) (Figure 9g).

PEG-APBA/GL networks only formed at pH > p $K_{\rm al,ester}$  as both of the APBA esters described above are sp<sup>3</sup>-hybridized, consistent with our hypothesis for other boronic acids. Further, PEG-APBA/GL formed networks under more acidic conditions (pH 4; Figure 9c) than PEG-PBA/GL (pH 6; Figure 4a), owing to the increased acidity of APBA relative to PBA (p $K_{\rm al,APBA}$  = 6.5 and p $K_{\rm a,PBA}$  = 7.9).<sup>20</sup> Our DFT calculations indicated that p $K_{\rm al}$  for the APBA/GL ester was 3 in comparison with 5.2 for the p $K_{\rm a}$  of the PBA/GL ester. The difference in p $K_{\rm a,ester}$  (2.2 units) led to a concomitant shift (2 units) in the onset of network formation.

At low pH, PEG-APBA/GL exhibited similar molecular behavior to PEG-PBA/GL. In PEG-APBA/GL,  $\Delta G_{\rm b}^{\ddagger}$  increased monotonically between pH 4 and 7, with a minimum in  $\Delta H_{\rm b}^{\ddagger}$  at pH 5 and a mostly negative  $\Delta S_{\rm b}^{\ddagger}$  (Figure 9d–f). These trends were similar to PEG-PBA/GL (Figure 6c–e), indicating that the reaction mechanisms at low pH were similar for these two systems. We hypothesized that at low pH (p $K_{\rm al,ester}$  = 3.0 < pH < p $K_{\rm al,APBA}$  = 6.5), network formation followed path 1B for PEG-APBA/GL (Figure 9g). Under these conditions, the nitrogen in APBA is fully protonated and does not interact with the neutral boron. This could explain how APBA at low pH behaves similarly to PBA, which lacks a nitrogen center.

The behavior of the PEG-APBA/GL networks changed at pH > p $K_{a1,APBA}$  = 6.5. The dynamics,  $\tau_R$ , reached a plateau (10–20 s) from pH 8 to 10 (Figure 9d). Further, the trends in the activation energies were reversed at higher pH.  $\Delta S_b^{\ddagger}$  became positive at pH > 6.5, reaching a maximum of 112 J  $K^{-1}$  mol<sup>-1</sup> at pH 9.5. At the same pH,  $\Delta H_b^{\ddagger}$  peaked at 112 kJ mol<sup>-1</sup> (Figure 9e,f). These reversals implied a mechanistic change for boronic ester formation around p $K_{a1,APBA}$  = 6.5. We propose that network formation for PEG-APBA/GL shifts from path 1B to path 2 near pH 6.5 (Figure 9g). In path 2, the boron is hydroxylated and negatively charged and, as such, interacts with the positively charged nitrogen. In the "loose-bolt" postulate, the deprotonated nitrogen center interacts with boron through solvent insertion. This was consistent with the

positive values of  $\Delta S_{\rm b}^{\ddagger}$  that we observed, alluding to a disordered transition state (as high entropy could arise from the presence of such inserted solvents). In addition, the "loose-bolt" postulate proposes neutral, high energy intermediates. This was consistent with the observed plateau of  $\Delta G_{\rm b}^{\ddagger}$  as a function of pH (as the energy of these neutral species is not expected to vary strongly with pH).

As pH was further increased, we observed a decrease in  $G_p$ for the PEG-APBA/GL networks around pH 9.5 (Figure 9c). Again, this deviated from the "charge rule", which predicts that the "optimal" conditions for boronic ester formation is pH 9.25 (eq 5), the minimum of  $G_p$  (2.3 kPa) for the APBA/GL networks (Figure 9c). At this pH, the pronation state of the reactants favors relatively unreactive species: the diols in GL are all protonated, the boron in APBA is hydroxylated, and the proximal nitrogen is protonated (meaning that there are no oxyanions, trigonal boron centers, or nitrogen lone pairs available to react). Additionally, pH 9.25 is situated between the p $K_a$  of the boron (p $K_{a1,APBA} = 6.5$ ) and the nitrogen (p $K_{a2}$  $\approx$  11). The presence of all these charged species would increase the energy required to produce neutral intermediates (such as those proposed by the "loose-bolt" postulate). 22 Robust networks formed again at pH > 10 (Figure 9c). At basic pH, the APBA/GL esters formed readily via path 3, as the proximal amine is deprotonated and its lone pair increases the reactivity of APBA (Figure 9g). Additionally, the diols in GL begin to deprotonate at pH > p $K_{al,GL} \approx 12$ , increasing the reactivity of the system.

In total, our rheometric analysis within ideal PEG-APBA/GL networks elucidated the reaction mechanism and activation energies of the APBA/GL junctions. Distinct ranges of pH corresponded to specific reaction pathways (Figure 9c–g). (1) At low pH (p $K_{\rm al,ester}=3.0$  < pH < p $K_{\rm al,APBA}=6.5$ ), PEG-APBA/GL behaved similarly to PEG-PBA/GL with network formation via path 1B. (2) At intermediate pH (p $K_{\rm al,APBA}=6.5$  < pH < p $K_{\rm a2}\approx11$ ), the reaction mechanism for APBA/GL shifted to path 2. (3) At high pH (p $K_{\rm a2}\approx11$  < pH), a new APBA/GL ester species formed and network formation followed path 3. Our reaction analysis supports the "loose-bolt" postulate for APBA/GL and Wulff-type boronic acids generally.

#### CONCLUSION

Through this work, we linked the macroscopic properties of dynamic covalent networks (DCvNs) to the molecular behavior at their junctions. By studying ideal boronic esterbased DCvNs, we showed how their mechanical properties, unobscured by the presence of defects, arise from the underlying chemistry. We connected viscoelasticity, as measured by shear rheometry, to the kinetics and thermodynamics of the dynamic junction, quantified via fluorescencebased spectroscopy, NMR spectroscopy, and DFT calculations. Further, we combined shear rheometry with Transition State Theory to quantitate the kinetics and thermodynamics of the network rearrangements, enabling a mechanistic understanding of boronic ester chemistry and elucidating reaction pathways for dynamic covalent chemistries. This approach corroborated the "loose-bolt" postulate for the reaction mechanism for Wulff-type boronic acids.

While our method to understand how macroscopic behavior arises from the chemistry at the reversible bond was developed for ideal DCvNs based on boronic ester chemistries, the general approach can be applied more broadly to other dynamic covalent networks. The method integrates chemical, mechanical, and theoretical analyses, which are not inherently restricted to any specific class of dynamic chemistry. We are confident that the method elaborated in this work can be applied to understand the behavior of other reversible addition networks, exploiting a similar approach using ideal dynamic covalent networks but with other cross-linking chemistries, e.g., hydrazone or oxime bonds. Further, the method will likely also aid in the study of dynamic exchange networks, as these reactions are generally sensitive to environmental conditions, affecting the dynamic rheology of the formed networks. In addition, while the use of ideal networks simplifies the study of how molecular details impact macroscale properties in reversible polymer networks, similar approaches can be applied to nonideal networks. Here, it may be necessary to account for a dispersion of Maxwell model elements or other rheological model frameworks to link chemistry to network properties. In total, we believe that the concept of using careful chemical analyses coupled with detailed rheological analysis will advance our understanding of dynamic polymer networks, improving our ability to predict, design, and leverage their unique properties for future applications.

## ASSOCIATED CONTENT

# Supporting Information

The Supporting Information is available free of charge at https://pubs.acs.org/doi/10.1021/jacs.0c06192.

Synthesis, sample preparation, computational and experimental methods, and model descriptions (PDF)

#### AUTHOR INFORMATION

# **Corresponding Author**

Mark W. Tibbitt — Macromolecular Engineering Laboratory and Department of Mechanical and Process Engineering, ETH Zurich, 8092 Zurich, Switzerland; o orcid.org/0000-0002-4917-7187; Phone: +41 44 632 25 16; Email: mtibbitt@ethz.ch

#### **Authors**

Bruno Marco-Dufort — Macromolecular Engineering Laboratory and Department of Mechanical and Process Engineering, ETH Zurich, 8092 Zurich, Switzerland; orcid.org/0000-0001-9098-9964

Ramon Iten – Macromolecular Engineering Laboratory and Department of Mechanical and Process Engineering, ETH Zurich, 8092 Zurich, Switzerland

Complete contact information is available at: https://pubs.acs.org/10.1021/jacs.0c06192

#### Notes

The authors declare no competing financial interest.

# ACKNOWLEDGMENTS

This work was supported by startup funds from ETH Zurich and the Claude & Giuliana Foundation.

# ABBREVIATIONS

DCvN, dynamic covalent network; DA, Diels—Alder; DFT, Density Functional Theory; PEG, poly(ethylene glycol); PBA, phenylboronic acid; APBA, *ortho*-aminomethylphenylboronic acid; GL, gluconolactone; ND, nitrodopamine; EXSY, 2D <sup>1</sup>H NMR exchange spectroscopy; M<sub>n</sub>, number average molecular

weight;  $G_p$ , plateau modulus;  $\tau_R$ , relaxation time;  $G'(\omega)$ , storage modulus;  $G''(\omega)$ , loss modulus;  $\omega$ , angular frequency;  $\omega_c$ , crossover frequency;  $\gamma$ , strain;  $\nu$ , concentration of elastically active network strands;  $\mu$ , total concentration of cross-links; R, gas constant; T, temperature; c, concentration of functional groups;  $K_{eq}$ , equilibrium constant; p, fraction of formed cross-links (or conversion);  $p_c$ , critical fraction of formed cross-links required to form a network;  $K_{eq,c}$ , critical equilibrium constant; wt%, total polymer concentration expressed in percent by weight;  $\Delta_r G^\circ$ , reaction Gibbs free energy;  $\tau_B$ , lifetime of the bond;  $k_b$  forward reaction rate constant;  $k_b$ , backward reaction rate constant; reverse magnetization exchange rate constants,  $k_b'$ ;  $t_{geb}$  gelation time;  $\Delta G_b^{\ddagger}$ , backward activation Gibbs free energy;  $\Delta H_b^{\ddagger}$ , backward activation enthalpy;  $\Delta S_b^{\ddagger}$ , backward activation entropy;  $k_B$ , Boltzmann constant; h, Planck constant

# REFERENCES

- (1) Rowan, S. J.; Cousins, G. R. L.; Stoddart, J. F.; Cantrill, S. J.; Sanders, J. K. M. Dynamic Covalent Chemistry. *Angew. Chem., Int. Ed.* **2002**, *41*, 898–952.
- (2) Kloxin, C. J.; Bowman, C. N. Covalent Adaptable Networks: Smart, Reconfigurable and Responsive Network Systems. *Chem. Soc. Rev.* **2013**, *42*, 7161–7173.
- (3) Montarnal, D.; Capelot, M.; Tournilhac, F.; Leibler, L. Silica-like Malleable Materials from Permanent Organic Networks. *Science* **2011**, 334, 965–968.
- (4) Chen, X.; Dam, M. A.; Ono, K.; Mal, A.; Shen, H.; Nutt, S. R.; Sheran, K.; Wudl, F. A Thermally Re-Mendable Cross-Linked Polymeric Material. *Science* **2002**, 295, 1698–1702.
- (5) Fairbanks, B. D.; Singh, S. P.; Bowman, C. N.; Anseth, K. S. Photodegradable, Photoadaptable Hydrogels via Radical-Mediated Disulfide Fragmentation Reaction. *Macromolecules* **2011**, 44, 2444–2450.
- (6) Webber, M. J.; Appel, E. A.; Meijer, E. W.; Langer, R. Supramolecular Biomaterials. *Nat. Mater.* **2016**, *15*, 13–26.
- (7) Smithmyer, M. E.; Deng, C. C.; Cassel, S. E.; Levalley, P. J.; Sumerlin, B. S.; Kloxin, A. M. Self-Healing Boronic Acid-Based Hydrogels for 3D Co-Cultures. *ACS Macro Lett.* **2018**, *7*, 1105–1110. (8) Yu, J.; Wang, J.; Zhang, Y.; Chen, G.; Mao, W.; Ye, Y.; Kahkoska, A. R.; Buse, J. B.; Langer, R.; Gu, Z. Glucose-Responsive Insulin Patch for the Regulation of Blood Glucose in Mice and Minipigs. *Nat. Biomed. Eng.* **2020**, *4*, 499–506.
- (9) Marco-Dufort, B.; Tibbitt, M. W. Design of Moldable Hydrogels for Biomedical Applications Using Dynamic Covalent Boronic Esters. *Mater. Today Chem.* **2019**, *12*, 16–33.
- (10) Zhong, M.; Wang, R.; Kawamoto, K.; Olsen, B. D.; Johnson, J. A. Quantifying the Impact of Molecular Defects on Polymer Network Elasticity. *Science* **2016**, 353, 1264–1268.
- (11) Leibler, L.; Rubinstein, M.; Colby, R. H. Dynamics of Reversible Networks. *Macromolecules* **1991**, 24, 4701–4707.
- (12) Semenov, A. N.; Rubinstein, M. Thermoreversible Gelation in Solutions of Associative Polymers. 1. Statics. *Macromolecules* **1998**, *31*, 1373–1385.
- (13) Rubinstein, M.; Semenov, A. N. Thermoreversible Gelation in Solutions of Associating Polymers. 2. Linear Dynamics. *Macromolecules* **1998**, *31*, 1386–1397.
- (14) Sheridan, R. J.; Bowman, C. N. A Simple Relationship Relating Linear Viscoelastic Properties and Chemical Structure in a Model Diels-Alder Polymer Network. *Macromolecules* **2012**, *45*, 7634–7641.
- (15) Winne, J. M.; Leibler, L.; Du Prez, F. E. Dynamic Covalent Chemistry in Polymer Networks: A Mechanistic Perspective. *Polym. Chem.* **2019**, *10*, 6091–6108.
- (16) Yount, W. C.; Loveless, D. M.; Craig, S. L. Small-Molecule Dynamics and Mechanisms Underlying the Macroscopic Mechanical Properties of Coordinatively Cross-Linked Polymer Networks. *J. Am. Chem. Soc.* **2005**, 127, 14488–14496.

- (17) Cromwell, O. R.; Chung, J.; Guan, Z. Malleable and Self-Healing Covalent Polymer Networks through Tunable Dynamic Boronic Ester Bonds. J. Am. Chem. Soc. 2015, 137, 6492–6495.
- (18) Hild, G. Model Networks Based on "endlinking" Processes: Synthesis, Structure and Properties. *Prog. Polym. Sci.* **1998**, 23, 1019—1149.
- (19) Parada, G. A.; Zhao, X. Ideal Reversible Polymer Networks. Soft Matter 2018, 14, 5186–5196.
- (20) Yesilyurt, V.; Webber, M. J.; Appel, E. A.; Godwin, C.; Langer, R.; Anderson, D. G. Injectable Self-Healing Glucose-Responsive Hydrogels with PH-Regulated Mechanical Properties. *Adv. Mater.* **2016**, 28, 86–91.
- (21) Yesilyurt, V.; Ayoob, A. M.; Appel, E. A.; Borenstein, J. T.; Langer, R.; Anderson, D. G. Mixed Reversible Covalent Crosslink Kinetics Enable Precise, Hierarchical Mechanical Tuning of Hydrogel Networks. *Adv. Mater.* **2017**, *29*, 1605947.
- (22) Sun, X.; Chapin, B. M.; Metola, P.; Collins, B.; Wang, B.; James, T. D.; Anslyn, E. V. The Mechanisms of Boronate Ester Formation and Fluorescent Turn-on in Ortho-Aminomethylphenylboronic Acids. *Nat. Chem.* **2019**, *11*, 768–778.
- (23) Grindy, S. C.; Learsch, R.; Mozhdehi, D.; Cheng, J.; Barrett, D. G.; Guan, Z.; Messersmith, P. B.; Holten-Andersen, N. Control of Hierarchical Polymer Mechanics with Bioinspired Metal-Coordination Dynamics. *Nat. Mater.* **2015**, *14*, 1210–1216.
- (24) Nishi, K.; Fujii, K.; Katsumoto, Y.; Sakai, T.; Shibayama, M. Kinetic Aspect on Gelation Mechanism of Tetra-Peg Hydrogel. *Macromolecules* **2014**, *47*, 3274–3281.
- (25) Tang, S.; Olsen, B. D. Relaxation Processes in Supramolecular Metallogels Based on Histidine-Nickel Coordination Bonds. *Macromolecules* **2016**, *49*, 9163–9175.
- (26) Mezger, T. G. The Rheology Handbook, 2nd ed.; Vincentz Network: Hannover, 2006.
- (27) Rubinstein, M.; Colby, R. H. *Polymer Physics*, 1st ed.; Oxford University Press: Oxford, 2003.
- (28) Tang, S.; Ma, H.; Tu, H. C.; Wang, H. R.; Lin, P. C.; Anseth, K. S. Adaptable Fast Relaxing Boronate-Based Hydrogels for Probing Cell-Matrix Interactions. *Adv. Sci.* **2018**, *5*, 1800638.
- (29) Akagi, Y.; Matsunaga, T.; Shibayama, M.; Chung, U.; Sakai, T. Evaluation of Topological Defects in Tetra-PEG Gels. *Macromolecules* **2010**, *43*, 488–493.
- (30) Stockmayer, W. H. Theory of Molecular Size Distribution and Gel Formation in Branched-Chain Polymers. *J. Chem. Phys.* **1943**, *11*, 45–55.
- (31) Brooks, W. L. A.; Deng, C. C.; Sumerlin, B. S. Structure-Reactivity Relationships in Boronic Acid-Diol Complexation. *ACS Omega* **2018**, *3*, 17863–17870.
- (32) Figueiredo, T.; Cosenza, V.; Ogawa, Y.; Jeacomine, I.; Vallet, A.; Ortega, S.; Michel, R.; Olsson, J. D. M.; Gerfaud, T.; Boiteau, J.-G.; Jing, J.; Harris, C.; Auzély-Velty, R. Boronic Acid and Diol-Containing Polymers: How to Choose the Correct Couple to Form "Strong" Hydrogels at Physiological PH. Soft Matter 2020, 16, 3628—3641.
- (33) Van Duin, M.; Peters, J. A.; Kieboom, A. P. G.; Van Bekkum, H. Studies on Borate Esters 1. The Ph Dependence of the Stability of Esters of Boric Acid and Borate in Aqueous Medium as Studied by 11B NMR. *Tetrahedron* **1984**, *40*, 2901–2911.
- (34) Peters, J. A. Interactions between Boric Acid Derivatives and Saccharides in Aqueous Media: Structures and Stabilities of Resulting Esters. *Coord. Chem. Rev.* **2014**, 268, 1–22.
- (35) Hall, D. G. Structure, Properties, and Preparation of Boronic Acid Derivatives. Overview of Their Reactions and Applications. In Boronic Acids: Preparation and Applications in Organic Synthesis and Medicine; Hall, D. G., Ed.; John Wiley and Sons: 2006; pp 1–99.
- (36) Rietjens, M.; Steenbergen, P. A. Crosslinking Mechanism of Boric Acid with Diols Revisited. *Eur. J. Inorg. Chem.* **2005**, 2005, 1162–1174.
- (37) Polgar, L. M.; Kingma, A.; Roelfs, M.; van Essen, M.; van Duin, M.; Picchioni, F. Kinetics of Cross-Linking and de-Cross-Linking of

- EPM Rubber with Thermoreversible Diels-Alder Chemistry. Eur. Polym. J. 2017, 90, 150–161.
- (38) McKinnon, D. D.; Domaille, D. W.; Cha, J. N.; Anseth, K. S. Bis-Aliphatic Hydrazone-Linked Hydrogels Form Most Rapidly at Physiological PH: Identifying the Origin of Hydrogel Properties with Small Molecule Kinetic Studies. *Chem. Mater.* **2014**, *26*, 2382–2387.
- (39) Yan, J.; Springsteen, G.; Deeter, S.; Wang, B. The Relationship among PK a, PH, and Binding Constants in the Interactions between Boronic Acids and Diols It Is Not as Simple as It Appears. *Tetrahedron* **2004**, *60*, 11205–11209.
- (40) Bosch, L. I.; Fyles, T. M.; James, T. D. Binary and Ternary Phenylboronic Acid Complexes with Saccharides and Lewis Bases. *Tetrahedron* **2004**, *60*, 11175–11190.
- (41) Furikado, Y.; Nagahata, T.; Okamoto, T.; Sugaya, T.; Iwatsuki, S.; Inamo, M.; Takagi, H. D.; Odani, A.; Ishihara, K. Universal Reaction Mechanism of Boronic Acids with Diols in Aqueous Solution: Kinetics and the Basic Concept of a Conditional Formation Constant. *Chem. Eur. J.* **2014**, *20*, 13194–13202.
- (42) Pross, A. Theoretical and Physical Principles of Organic Reactivity; John Wiley and Sons: 1995.
- (43) Li, H.; Li, H.; Dai, Q.; Li, H.; Brédas, J.-L. Hydrolytic Stability of Boronate Ester-Linked Covalent Organic Frameworks. *Adv. Theory Simulations* **2018**, *1*, 1700015.
- (44) Ogden, W. A.; Guan, Z. Recyclable, Strong, and Highly Malleable Thermosets Based on Boroxine Networks. *J. Am. Chem. Soc.* **2018**, *140*, 6217–6220.
- (45) Monajemi, H.; Cheah, M. H.; Lee, V. S.; Zain, S. M.; Tajuddin Wan Abdullah, W. A. On the Kinetics and Reaction Mechanisms of Boronic Acid in Interaction with Diols for Non-Enzymatic Glucose Monitoring Applications: A Hybrid DFT Study. *RSC Adv.* **2014**, *4*, 10505–10513.
- (46) Ishihara, K.; Mouri, Y.; Funahashi, S.; Tanaka, M. Mechanistic Study of the Complex Formation of Boric Acid. *Inorg. Chem.* **1991**, 30, 2356–2360.
- (47) Kagawa, S.; Sugimoto, K. I.; Funahashi, S. Kinetic Study on Complexation of Boric Acid with 4-Isopropyltropolone in Non-Aqueous Solvents. *Inorg. Chim. Acta* 1995, 231, 115–119.
- (48) Mahmad Rasid, I.; Ramirez, J.; Olsen, B. D.; Holten-Andersen, N. Understanding the Molecular Origin of Shear Thinning in Associative Polymers through Quantification of Bond Dissociation under Shear. *Phys. Rev. Mater.* **2020**, *4*, 55602.
- (49) Liu, Z.; He, H. Synthesis and Applications of Boronate Affinity Materials: From Class Selectivity to Biomimetic Specificity. *Acc. Chem. Res.* **2017**, *50*, 2185–2193.
- (50) Wulff, G.; Lauer, M.; Böhnke, H. Rapid Proton Transfer as Cause of an Unusually Large Neighboring Group Effect. *Angew. Chem., Int. Ed. Engl.* **1984**, 23, 741–742.
- (51) Brooks, W. L. A.; Sumerlin, B. S. Synthesis and Applications of Boronic Acid-Containing Polymers: From Materials to Medicine. *Chem. Rev.* **2016**, *116*, 1375–1397.